Cancer Biol Med 2026. doi: 10.20892/j.issn.2095-3941.2025.0775

ORIGINAL ARTICLE

Metabolic engineering of SLC38A2 reprograms glutamine utilization and enhances CAR-macrophage antitumor function in solid tumors

Mingzhu Liu[1,2,3,4,5], Qingxi Chen[3,4], Luoling Zhang[3,4], Yunxuan Zhou[3,4], Ning Wen[3,4], Jin Jin[6], Junchao Cai[7], Shicheng Su[1,2], Jiang Li[1,2], Qiyi Zhao[3,4,5]

[1]Guangdong Provincial Key Laboratory of Malignant Tumor Epigenetics and Gene Regulation, Medical Research Center, Sun Yat-sen Memorial Hospital, Sun Yat-sen University, Guangzhou 510120, China; [2]Breast Tumor Center, Sun Yat-sen Memorial Hospital, Sun Yat-sen University, Guangzhou 510120, China; [3]Department of Infectious Diseases, The Third Affiliated Hospital, Sun Yat-sen University, Guangzhou 510630, China; [4]Guangdong Provincial Key Laboratory of Liver Disease Research, The Third Affiliated Hospital, Sun Yat-sen University, Guangzhou 510630, China; [5]Laboratory of Clinical Microbiology, The Third Affiliated Hospital of Sun Yat-sen University, Guangzhou 510630, China; [6]Center for Neuroimmunology and Health Longevity, The Third Affiliated Hospital, Sun Yat-sen University, Guangzhou 510630, China; [7]Department of Immunology, Zhongshan School of Medicine, Sun Yat-sen University, Guangzhou 510080, China

ABSTRACT

Objective: This study was aimed at investigating metabolic dysregulation in tumor-associated macrophages (TAMs) in breast cancer and developing a metabolically enhanced chimeric antigen receptor macrophage (CAR-M) strategy to boost antitumor potency in solid tumors.

Methods: Integrated scRNA-seq and metabolomic analyses were performed to characterize metabolic alterations in macrophages within the breast cancer tumor microenvironment (TME). According to the identified metabolic vulnerabilities, SLC38A2-overexpressing anti-HER2 CAR-Ms were engineered. Glutamine uptake and phagocytic activity were assessed to evaluate functional enhancement.

Results: TAMs in breast cancer exhibited substantial metabolic dysregulation, particularly impaired glutamine metabolism accompanied by decreased expression of the glutamine transporter SLC38A2. Overexpression of SLC38A2 in anti-HER2 CAR-Ms, compared with conventional anti-HER2 CAR-Ms, enhanced glutamine uptake and markedly augmented phagocytosis of $HER2^+$ breast cancer cells.

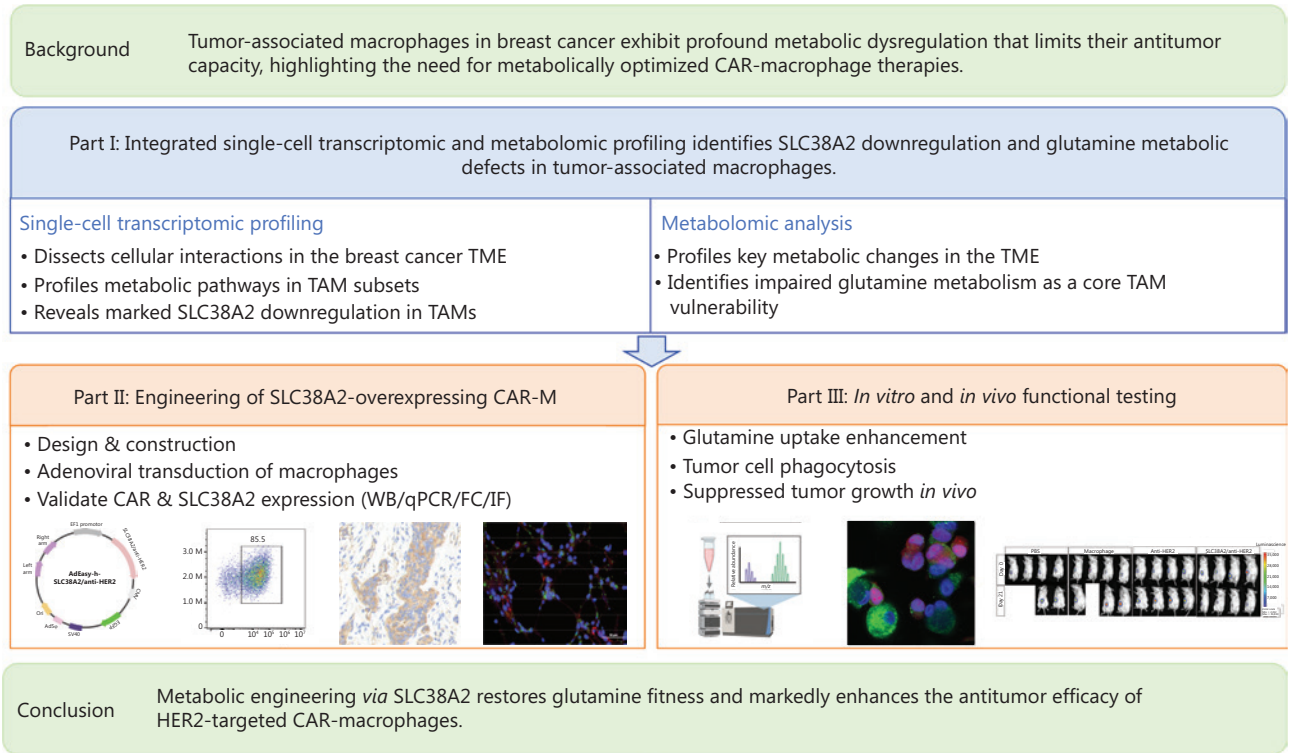
Conclusions: Metabolic engineering *via* SLC38A2 restored glutamine fitness and enhanced the antitumor activity of HER2-targeted CAR-Ms, thus providing a promising strategy to boost CAR-M–mediated tumor suppression in solid tumors.

KEYWORDS CAR-macrophage; metabolic engineering; SLC38A2; glutamine metabolism

Introduction

The rapid emergence of chimeric antigen receptor (CAR) macrophage (CAR-M) therapies has ushered in a new era in cancer immunotherapy[1,2]. Macrophages, the most abundant innate immune cells infiltrating the tumor microenvironment (TME), have a strong intrinsic ability to penetrate deep into tumor tissues and directly eliminate cancer cells through phagocytosis[3,4]. Moreover, macrophages can enhance tumor antigen presentation, thereby mitigating tumor heterogeneity and sustaining downstream T-cell activation, and ultimately orchestrating broader antitumor immune responses[5-7]. Arming macrophages with refined next generation CAR designs can help overcome key roadblocks and permit fine tuning of antitumor immunity[7]. Recent clinical studies have demonstrated the feasibility, safety, and preliminary antitumor activity of CAR-Ms in patients with solid tumors such as breast cancers[8,9]. In parallel, advances in stem cell biology have enabled the generation of CAR-engineered macrophages from human pluripotent stem cells, thus providing a scalable and standardized cellular source for CAR-M therapies[10].

Corresponding to: Qiyi Zhao
E-mail: zhaoqyi@mail.sysu.edu.cn
ORCID ID: https://orcid.org/0000-0003-0649-0437
Received December 7, 2025; accepted March 2, 2026;
published online April 1, 2026.
Available at www.cancerbiomed.org
©2026 The Authors. Creative Commons Attribution-NonCommercial 4.0 International License (CC BY-NC 4.0)



Study flowchart Part I integrated single-cell transcriptomic and metabolomic profiling to reveal cellular interactions in the breast cancer tumor microenvironment, characterize metabolic programs across TAM subsets, and identify marked downregulation of the glutamine transporter SLC38A2 alongside extensive glutamine metabolic defects. These analyses revealed impaired glutamine utilization as a central metabolic vulnerability of tumor-associated macrophages. Part II engineered metabolically enhanced HER2-targeted CAR-macrophages by overexpressing SLC38A2. This part included CAR construct design; adenoviral transduction of macrophages; and validation of CAR and SLC38A2 expression *via* western blotting, qPCR, flow cytometry, and immunofluorescence. Part III assessed the functional consequences of SLC38A2 overexpression. *In vitro* assays demonstrated greater glutamine uptake and markedly greater phagocytosis of $HER2^+$ tumor cells by SLC38A2-overexpressing CAR-Ms than conventional CAR-Ms. These enhanced functional activities translated to *in vivo* results indicating that SLC38A2/anti-HER2 CAR-M treatment significantly suppressed tumor growth in $HER2^+$ tumor-bearing mice. Collectively, these findings established that metabolic engineering *via* SLC38A2 restored glutamine fitness and markedly augmented the antitumor efficacy of HER2-targeted CAR-macrophages. CAR-M, chimeric antigen receptor macrophage; TAM, tumor-associated macrophage; TME, tumor microenvironment; WB, western blotting; qPCR, quantitative PCR; FC, flow cytometry; IF, immunofluorescence.

CAR-Ms represent a major advancement in immunotherapy, particularly for treating solid tumors, in which traditional CAR-T therapies face limitations[8,11-14]. Difficulties arise in the use of CAR-T therapies in solid tumors, including limited trafficking into and retention within densely fibrotic tumor stroma, dampened effector activity in highly immunosuppressive niches, and restricted access to tumor cells embedded within complex tissue architectures[15,16]. Although macrophages can inherently infiltrate into solid tumors, the application of CAR-M therapies to solid tumors still faces challenges including immunological barriers and extensive metabolic constraints within the TME[2,11,17]. Current strategies to enhance CAR-M functionality focus on multiple fronts. One approach involves *in vitro* pre-stimulation to augment proinflammatory activation[18,19]. Other strategies include advances in CAR gene delivery technologies, such as optimized viral vectors and non-viral platforms including lipid nanoparticles[20,21]. Although these advances have strengthened CAR expression and activation in engineered macrophages, thereby highlighting the therapeutic promise of CAR-Ms, they still fall short of addressing the decisive effects of the tumor metabolic landscape on CAR-M persistence and therapeutic efficacy[22,23]. Therefore, elucidating how the TME reshapes macrophage phenotypes and identifying new targets to enhance CAR-M function are urgently needed.

The TME reprograms CAR-Ms through the release of immunosuppressive factors and metabolic cues[17,24] that drive macrophage polarization toward a pro-tumoral phenotype and thereby compromise their antitumor function. The intricate metabolic crosstalk between immune cells and tumor

cells has emerged as a critical determinant of immunotherapy response[17,25-28]. Multiple potential metabolic crosstalk mechanisms have been reported, including nutrient competition, immunomodulatory effects of metabolites, and metabolic adaptability[29-32]. Notably, metabolic regulators, in conjunction with epigenetic modifiers and surface receptors, have emerged as key determinants of both myeloid and lymphoid cell behavior, and are increasingly incorporated into the design of next generation CAR-based immunotherapies[2]. Nevertheless, little is known regarding how metabolic cues in the TME regulate CAR-M functions. Therefore, elucidating the specific mechanisms through which the TME reshapes macrophage metabolism is expected to provide valuable insights for optimizing CAR-M therapeutic strategies.

Herein, by integrating single-cell transcriptomic and metabolomic profiling, we identified glutamine metabolism as a key vulnerability of macrophages in the TME. Leveraging this mechanistic insight, we engineered metabolically empowered CAR-Ms with markedly enhanced phagocytic and antitumor activity *in vitro*. Importantly, these metabolic enhancements translated to marked tumor growth suppression in $HER2^+$ tumor bearing mouse models, thus providing a metabolism informed strategy to enhance the efficacy of CAR-M immunotherapy in solid tumors.

Materials and methods

Single-cell RNA-seq data processing and cell-cell communication analysis

The published single-cell RNA-seq dataset GSE155109 was downloaded from the Gene Expression Omnibus (GEO) database and processed in Seurat (v5), including quality control, normalization, dimensionality reduction, clustering, and uniform manifold approximation and projection (UMAP) visualization. Major cell populations were annotated according to canonical marker genes and verified with reference based mapping with the SingleR package. Cell-cell communication between immune cells and cancer cells was inferred with CellChat through construction of ligand-receptor interaction networks and identification of enriched signaling pathways. Gene Ontology (GO) enrichment analysis using the clusterProfiler package was performed on cluster-specific marker genes to explore biological functions associated with distinct immune subsets. All analyses were conducted in R with default parameters, unless otherwise specified.

Metabolomic analysis

Raw metabolite intensities were obtained from the publicly available metabolomics dataset MTBLS11091 (MetaboLights, https://www.ebi.ac.uk/metabolights/). Tissue-level metabolomic data used in this study were obtained from the processed and annotated metabolite matrices from a prior study (PMID: 35105939). Raw metabolite intensities were $\log_2$-transformed and normalized before downstream analysis. Differentially expressed metabolites between groups were identified according to thresholds of $\log_2FC > 1$ or $\log_2FC < -1$ combined with FDR < 0.05. Significantly enriched metabolites were visualized in a volcano plot.

For pathway level interpretation, differentially expressed metabolites were subjected to functional enrichment analysis with MetaboAnalyst 6.0 (https://new.metaboanalyst.ca/MetaboAnalyst/). Both overrepresentation analysis and topology analysis were applied to identify significantly perturbed metabolic pathways across experimental conditions.

Metabolic activity assessment of macrophages with the scMetabolism pipeline

Single-cell metabolic activity was quantified with the scMetabolism R package. Raw gene expression data were first extracted from the Seurat object and normalized with Seurat's default workflow. The subset of cells annotated as macrophages was subjected to downstream metabolic analysis. To evaluate pathway-level metabolic programs, we applied the scMetabolism score function with the KEGG based pathway gene sets embedded in the package. For each macrophage, enrichment scores representing the activity of individual metabolic pathways were calculated with the AUCell algorithm. Default parameters were applied, unless otherwise specified. The resulting cell-by-pathway metabolic activity matrix was further scaled and visualized. Heatmaps were generated to display pathway activity across macrophage subpopulations with the pheatmap package.

Generation of SLC38A2/anti-HER2 macrophages

To generate macrophages expressing the SLC38A2-augmented anti-HER2 CAR, we first designed and optimized a HER2-targeting chimeric antigen receptor in SnapGene software. The CAR cassette consisted of a CD8 signal peptide, human anti-HER2 single-chain variable fragment (scFv), CD8 hinge, CD28 transmembrane region with partial intracellular motifs, and CD3ζ signaling domain. For control experiments, we constructed 2 negative control CAR variants encoding either the intracellular signaling domain alone (ICD-only) or the extracellular domain alone (ECD-only), to enable assessment of target specificity and signaling dependence. To enhance glutamine uptake ability, we incorporated the SLC38A2 gene, encoding a key glutamine transporter essential for macrophage metabolic fitness in the TME, directly

downstream of the anti-HER2 scFv, thereby generating a bifunctional CAR module capable of both HER2 recognition and metabolic augmentation. All constructs were linked *via* a T2A self-cleaving peptide. The complete CAR expression cassettes were synthesized and cloned into the pAdEasy-EF1-MCS-CMV-EGFP adenoviral vector. Vector integrity was verified through restriction digestion and Sanger sequencing. Adenoviral particles were subsequently used for macrophage transduction at a multiplicity of infection (MOI) of 500 plaque forming units, to establish stable expression of the SLC38A2/anti-HER2 CAR in macrophages. Macrophages transduced with an empty EGFP vector were designated as GFP-Ms and served as controls.

Real-time quantitative PCR

Total RNA was extracted with an Ambion RiboPure RNA Purification Kit (cat# AM1924, Thermo Fisher Scientific) and reverse transcribed into cDNA with iScript™ RT Supermix (cat# 1708841, Bio-Rad), according to the manufacturer's instructions. Quantitative PCR (qPCR) was performed with template cDNA, gene-specific primers, TaqMan Gene Expression Assays, and TaqMan Gene Expression Master Mix (cat# 4369016, Applied Biosystems). Human TaqMan assays for GAPDH (Hs02786624_G1) and SLC38A2 (Hs01089958_G1) were used. The primer sequences are listed in **Table S1**. Data were collected and analyzed with a LightCycler 480 instrument (Roche). Reactions were run according to the manufacturer's protocol, and relative gene expression levels were calculated with the $2^{-\Delta\Delta Ct}$ method with GAPDH as the endogenous control.

CD14$^+$ monocyte isolation and macrophage differentiation for CAR transduction

Peripheral blood was collected from healthy donors *via* venipuncture, and the peripheral blood mononuclear cell (PBMC) fraction was isolated with density gradient centrifugation. Briefly, 7.5 mL PBMC-containing buffy coat was diluted with 22.5 mL phosphate-buffered saline (PBS) and gently mixed. In a 50 mL centrifuge tube, 15 mL Ficoll-Paque (cat# 17144003) was carefully layered on, and the diluted buffy coat was slowly added on top to maintain a clear interface. Samples were centrifuged at 800*g* for 20 min at 22°C with minimal braking (0–1). After centrifugation, distinct layers were observed: the top plasma/PBS layer, the middle cloudy PBMC layer, and the bottom layer containing red blood cells and granulocytes. The PBMC layer was carefully collected, combined in a new 50 mL tube, diluted to 40 mL with PBS, and centrifuged at 800*g* for 5 min at room temperature. Cells were washed twice with PBS and counted with trypan blue to confirm a viability ≥70%. For CD14$^+$ monocyte isolation, PBMCs were resuspended in MACS Rinsing Solution Buffer (cat# 130-091-222) and filtered through a 40 μm strainer to remove cell aggregates. Cells were counted, centrifuged at 300*g* for 10 min, and resuspended at 1×10^7 cells per 80 μL buffer. CD14 MicroBeads (cat# 130-050-201) were added at 20 μL per 1×10^7 cells, mixed gently, and incubated for 15 min at 4°C. Cells were washed with 1–2 mL buffer per 1×10^7 cells, centrifuged at 300*g* for 10 min, and resuspended in 500 μL buffer per 1×10^8 cells. LS magnetic columns (cat# 130-042-401) were pre-wetted with 3 mL buffer and placed on a magnetic separator. The cell suspension was applied to the column and allowed to flow through, and the column was subsequently washed 3 times with 3 mL buffer. CD14$^+$ monocytes were eluted with 5 mL buffer with the aid of a plunger into a new 15 mL tube. Purified CD14$^+$ monocytes were seeded into ultra-low attachment 6-well plates and differentiated into macrophages by culture in RPMI-1640 supplemented with 10% fetal bovine serum (FBS) and 100 ng/mL Human M-CSF Recombinant Protein, PeproTech (cat# 300-25) for 5 days. Differentiation was monitored by light microscopy. On day 5, adenovirus was added at a multiplicity of infection of 1×10^3, on the basis of plaque forming units. Macrophages were harvested on day 7 and assessed for CAR expression, differentiation status, and purity with flow cytometry.

siRNA mediated gene silencing

Small interfering RNAs (siRNAs) targeting human SLC38A2 and a non-targeting negative control siRNA were designed and synthesized by Motif Biotech (Suzhou, China). Macrophages were transfected with siRNAs at a final concentration of 50 nM with Lipofectamine 3000 Reagent (Thermo Fisher Scientific, cat# L3000015) according to the manufacturer's instructions. Briefly, siRNAs and transfection reagent were separately diluted in Opti-MEM, then combined to form lipid-siRNA complexes before being added to the cells. After transfection, macrophages were cultured under standard conditions, and gene silencing efficiency was assessed at the mRNA and protein levels with qPCR and immunoblotting, respectively. Detailed sequences and information for all siRNAs used in this study are provided in **Table S2**.

Cell culture

Human primary macrophages were cultured in RPMI 1640 medium (Gibco, cat# 21870076) supplemented with 10% FBS (Thermo Scientific, cat# 10099-141) and 1% penicillin-streptomycin (Thermo Fisher Scientific, cat# 10378016). For glutamine deprivation experiments, macrophages were maintained in glutamine-free RPMI 1640 medium (Corning, cat# 15-040-CV) supplemented with 10% FBS and antibiotics, as indicated. The human breast cancer cell line MDA-MB-231 was cultured in high-glucose DMEM (Gibco, cat# C11995500BT)

supplemented with 10% FBS and 1% penicillin-streptomycin at 37°C in a humidified incubator under 5% CO_2. The human ovarian cancer cell line SKOV3 and the human breast cancer cell line SKBR3 were cultured in McCoy's 5A medium (Gibco, cat# 16600082) supplemented with 10% FBS and 1% penicillin-streptomycin under standard culture conditions.

Flow cytometry

For surface marker staining and flow cytometric analysis, cells were incubated with the following antibodies: Whitlow/218 linker recombinant rabbit mAb (Alexa Fluor® 647 conjugate; cat# S0B1796-50T, Starter), anti-SLC38A2 (cat# sc-166366, Santa Cruz), goat anti-mouse IgG (H+L) secondary antibody-PE (cat# M30004-1, Invitrogen) and anti-CD68 [Alexa Fluor® 488 anti-CD68 antibody (KP1); cat# ab222914, Abcam]. For intracellular staining, cells were first treated with an Intracellular Fixation and Permeabilization Kit (cat# 88-8824, eBioscience) according to the manufacturer's instructions. Stained samples were analyzed on a CytoFlex flow cytometer (Beckman Coulter), and data were processed in FlowJo software (v10, TreeStar).

Metabolite extraction from cell culture supernatants and LC-MS analysis

Cell culture supernatants were collected after incubation, and 500 μL samples were transferred into 1.5 mL centrifuge tubes. Samples were centrifuged at 13,000*g* for 10 min at 4°C to remove cellular debris. For metabolite extraction and protein precipitation, 200 μL clarified supernatant was mixed with 800 μL pre-chilled LC-MS grade methanol and vortexed thoroughly. The mixture was further vortexed at 2,000 rpm for 10 min to ensure efficient metabolite extraction. Protein precipitation was accelerated by incubation of the samples at −30°C for 1 h. The samples were then centrifuged at 14,000 rpm for 15 min at 4°C, and the supernatant was carefully transferred to a new tube. Approximately 850 μL supernatant was subjected to vacuum lyophilization at 4°C until completely dry. Dried samples were either stored at −20°C or immediately reconstituted for LC-MS analysis. For reconstitution, samples were resuspended in 100 μL 50% acetonitrile in water, vortexed for 30 s, and sonicated in a water bath for 3 min at room temperature. Insoluble material was removed by centrifugation at 14,000 rpm for 15 min at 4°C, and 80 μL clarified supernatant was carefully transferred into LC-MS vials with inserts, by avoiding any precipitate. Quality control (QC) samples were prepared by pooling equal volumes (5–10 μL, adjusted according to total sample volume) of all experimental samples to monitor instrument stability and data quality in untargeted metabolomics experiments; QC samples were optional for targeted analyses. LC-MS analysis was performed with an Agilent 1290 Infinity liquid chromatography system coupled to an Agilent 6470 triple quadrupole mass spectrometer (Agilent 1290-6470, low-resolution LC-MS) to profile metabolites in the cell culture supernatants.

Western blot analysis

Cell pellets from 1×10^6 cells were collected and lysed in 100 μL RIPA buffer (Beyotime, cat# P0013J) on ice for 30 min. Lysates were centrifuged at 14,000*g* for 30 min at 4°C, and supernatants were collected. Protein concentrations were determined with BCA assays (Thermo Scientific, cat# 23225). Approximately 10 μg total protein per sample was resolved by SDS-PAGE and transferred to membranes for immunoblotting. The following primary antibodies were used: GAPDH (MC4) mouse monoclonal antibody (Beijing Ray Antibody Biotech, cat# RM2002, 1:1,000), VDAC1 recombinant rabbit monoclonal antibody (Starter, cat# S-1877-18, 1:1,000), GLUD1 monoclonal antibody (Proteintech, cat# 67026-1-Ig, 1:1,000), GLS antibody (Abclonal, cat# A23189, 1:1,000), DRP1 (CST, cat# 570S, 1:1,000), and GOT2 monoclonal antibody (Proteintech, cat# 67738-1-Ig, 1:1,000). Goat anti-mouse IgG, light-chain specific antibody (HRP conjugate) (Cell Signaling Technology, cat# 91196, 1:2,000) was used for detection. Representative immunoblots were captured with a ChemiDoc Touch Imaging System (Bio-Rad).

Phagocytosis assays of CAR-Ms

The functionality of CAR-Ms was evaluated through co-culture with $HER2^-$ (MDA-MB-231) or $HER2^+$ (SKBR3) mCherry-expressing tumor cells. In each well of a 96-well plate (WHB-96-2), 2×10^3 tumor cells were mixed with CAR-Ms in 100 μL RPMI 1640 complete medium at an effector-to-target (E:T) ratio of 1:1. After 24 h of co-culture, phagocytic activity was assessed with flow cytometry and immunofluorescence imaging.

T cell proliferation assays

Autologous T cells were first labeled with 5 μM carboxyfluorescein succinimidyl ester (CFSE, Selleck Chemicals) for 25 min at 4°C. Labeled T cells were then pre-activated on plates coated with 2 μg/mL anti-CD3 (Biolegend) at 37°C under 5% CO_2 for 16–18 h. CAR-Ms used in the assay were previously co-cultured with tumor cells and subsequently isolated. At 3 days after T cell activation, T cells were co-cultured with the pretreated CAR-Ms at a T cell:macrophage ratio of 5:1 for 48 h. T cell proliferation was assessed with CFSE dilution and flow cytometry.

Detection of cytokine production by ELISA

Cytokine secretion by CAR-Ms was quantified with enzyme-linked immunosorbent assay (ELISA). Briefly, CAR-Ms were cocultured with $HER2^+$ SKOV3 tumor cells for 24 h under

standard culture conditions. After coculture, supernatants were collected and centrifuged to remove cellular debris.

The concentrations of human IL-10 and TNF-α in the culture supernatants were measured with commercially available ELISA kits (IL-10: cat# RAB0244; TNF-α: cat# DTA00D) according to the manufacturers' instructions. Briefly, standards and samples were added to pre-coated plates, then incubated with detection antibodies and enzyme conjugates. After substrate development, the reaction was stopped, and absorbance signals were measured with a Synergy H1 multimode microplate reader (BioTek). Cytokine concentrations were calculated according to standard curves generated for each assay.

Immunofluorescence

After blocking, cells were incubated overnight at 4°C with CD68 (E3O7V) rabbit monoclonal antibody (1: 500, cat# 97778, CST) and SLC38A2 (1:50, cat# sc-166366, Santa Cruz). After being washed, samples were incubated for 1 h at room temperature with Alexa Fluor™ 488-conjugated donkey anti-rat IgG (H+L) highly cross-adsorbed secondary antibody (1:300, cat# A21208, Thermo Fisher Scientific) and Alexa Fluor™ 594-conjugated donkey anti-mouse IgG (H+L) highly cross-adsorbed secondary antibody (1:300, cat# A21203, Thermo Fisher Scientific). For mitochondrial staining, cells were incubated with MitoTracker® Deep Red FM (cat# 40743ES50) according to the manufacturer's instructions before fixation. Nuclei were counterstained with DAPI (5 mg/mL, cat# D3571, Thermo Fisher Scientific). Confocal images were acquired with an Olympus FV3000 microscope.

Animal experiments and bioluminescence imaging

Female SGM3 mice (age 6–8 weeks) were used for all *in vivo* experiments. SKBR3 tumor cells stably expressing the luciferase (Luc) reporter were collected, centrifuged at 1,000*g* for 3 min, and washed 3 times with sterile PBS. Cells were then resuspended and mixed with 0.4% trypan blue to determine viable cell numbers under a microscope. Tumor cell suspensions were prepared at a concentration of 1×10^7 cells/mL, and 50 μL was subcutaneously injected into the flank in each mouse.

Tumor growth was monitored weekly with *in vivo* bioluminescence imaging (BLI). Mice were randomly assigned to experimental groups according to the average bioluminescence radiance, to ensure comparable initial tumor burden across groups. CAR-Ms were administered *via* tail vein injection at a dose of 3×10^6 cells per mouse. Tumor progression was monitored weekly with BLI to quantify tumor growth and treatment response. All animal procedures were performed in accordance with institutional guidelines and approved by the Institutional Animal Care and Use Committee of Sun Yat-sen University.

Statistical analysis

Data are presented as mean ± SD. Statistical significance between groups was analyzed with two-tailed Welch's *t*-test assuming unequal variances. For comparisons involving more than 2 groups, statistical significance was determined with one-way ANOVA followed by appropriate multiple-comparison tests. $P < 0.05$ was considered statistically significant. For multiple comparisons, *P* values were adjusted with the Holm method. Statistical analyses were performed in GraphPad Prism 10 or R 4.3.

Results

Single-cell transcriptomic analysis highlights the role of macrophage metabolic pathways in the TME

To comprehensively characterize the immune landscape of the TME in breast cancers, we used published scRNA-seq data (GSE155109) derived from tumor and matched nontumor tissues of 9 patients with early-stage breast cancer[33] (**Figure 1A**). After initial quality control and batch correction, we performed dimensionality reduction and clustering with UMAP. The UMAP visualization revealed distinct transcriptomic profiles between tumor and nontumor tissues (**Figure 1B**). We classified a total of 18,082 cells into 14 distinct cell types according to canonical lineage markers (**Figure 1C and 1D**). After characterizing the major cellular populations and their transcriptional heterogeneity, we next investigated intercellular communication within the TME. Using CellChat, we first examined cell-cell interactions between immune cells and cancer cells. Among all immune subsets, macrophages exhibited the strongest signaling crosstalk with cancer cells (**Figure 1E**). Similarly, analysis of intercellular communication among immune cell subsets revealed that macrophages were the dominant signaling hub, exhibiting the strongest ligand-receptor interactions with other immune cells (**Figure 1F**). Given the central role of macrophages in these intercellular communication networks, we next focused on clarifying their functions in the TME. Pathway enrichment analysis revealed that macrophages, beyond their well-known immune-related functions, showed notable enrichment in metabolic pathways, thus highlighting the critical roles of metabolism in shaping macrophage function within the TME (**Figure 1G**). Notably, comparative GO enrichment analyses across other immune cell subsets demonstrated less prominent metabolic pathway enrichment than observed in macrophages (**Figure S1A**). In parallel, scMetabolism-based KEGG pathway analyses further revealed

heterogeneous metabolic activity among immune cell populations, thus supporting prominent metabolic involvement of macrophages (**Figure S1B**).

Metabolomic profiling identifies glutamine as a key metabolic node of macrophages in the TME

To delineate the metabolic landscape of breast cancers and its relevance to macrophage function, we analyzed metabolomic profiles of tumor and adjacent normal breast tissues[34]. Systematic characterization revealed a marked metabolic divergence between tumor and normal samples (**Figure 2A**), which was accompanied by broad shifts in metabolite abundance (**Figure 2B**). Pathway enrichment analysis indicated that breast cancer tissues showed associations with alterations in amino acid-associated pathways, including alanine, aspartate, and glutamate metabolism; arginine biosynthesis; arginine and proline metabolism; β-alanine metabolism; and glutathione metabolism (**Figure 2C**).

To evaluate whether these tissue-level metabolic alterations might be recapitulated at the cellular level and influence immune cell-cancer cell interactions, we examined metabolic profiles with single-cell metabolomics (MTBLS11091)[35]. We first asked how these metabolic alterations might shape the metabolic behavior of immune cells, particularly macrophages, which are dominant immune regulators in the TME. We compared the metabolic profiles of macrophages *vs*. breast cancer cells. Macrophages and cancer cells exhibited markedly distinct metabolic signatures (**Figure 2D and 2E**). Notably, amino acid-associated pathways emerged as the most prominently altered metabolic processes (**Figure 2F**), thus reinforcing a shared, amino-acid-centered metabolic theme consistently observed across tissues, cancer cells, and macrophage analyses. Similarly to the observed tissue-level metabolic patterns, substantial metabolic divergence between breast cancer cells (MDA-MB-231 and MCF-7) and normal breast epithelial cells (MCF10A) was also found (**Figure S1A–S1C**), such that tumor cells displayed markedly elevated metabolic activity and enrichment in amino acid-associated pathways.

Because both tissue-level and cellular level metabolomic analyses consistently revealed pronounced metabolic reprogramming in breast cancers, we performed an integrated comparative analysis to identify key metabolites driving consistent metabolic divergence across these distinct metabolomic datasets. D-(-)-glutamine was identified as the most prominent shared metabolic feature (**Figure 2G**). Notably, the finding that glutamine-associated metabolites displayed markedly lower abundance in macrophages than tumor cells (**Figure 2H and 2I**) suggested that macrophages operate under a relative glutamine-restricted state within the TME.

The glutamine transporter SLC38A2 is downregulated in tumor-associated macrophages

To define the molecular basis underlying the glutamine-restricted state in macrophages within the breast TME, we re-clustered macrophages extracted from our single-cell transcriptomic dataset (**Figure 3A–3D**). Five transcriptionally distinct macrophage subpopulations were identified. Notably, tumor-associated macrophages were enriched predominantly in the Macrophages_1 subset, whereas normal breast tissue macrophages were represented primarily by the Macrophages_2 subset, thereby indicating a shift in macrophage composition during tumor progression. Using the scMetabolism pipeline to assess metabolic activity (**Figure 3E**), we observed robust metabolic heterogeneity across macrophage subsets. This cell-intrinsic metabolic feature was consistent with the above-mentioned tissue-level metabolomic profiling (**Figure 2G**), which revealed elevated glutamine consumption in breast cancer, a pattern largely driven by the high metabolic demand of proliferating cancer cells. In this context, macrophages in the TME exhibited comparatively lower glutamine availability despite the overall upregulation of glutamine metabolism in tumor tissues. To elucidate the underlying mechanism, we analyzed the expression of known glutamine transporters across macrophage subsets[36]. This comparative single-cell transcriptomic analysis revealed preferential SLC38A2 expression in macrophages derived from. normal breast tissue, with relatively higher expression in the Macrophages_2 subset than other immune cell populations; these findings suggested that SLC38A2 was the primary transporter mediating glutamine uptake in macrophages (**Figure 3F–3H**).

To further validate these findings in human tissues, we performed immunohistochemical analyses of primary breast cancer specimens, which demonstrated relatively higher SLC38A2 expression in adjacent nontumor regions than in tumor nests (**Figure 3I**). Consistently, immunofluorescence staining revealed colocalization of SLC38A2 with $CD68^+$ macrophages, with a trend toward a diminished SLC38A2 signal within tumor regions (**Figure 3J**). To determine whether the TME might actively suppress SLC38A2 expression in macrophages, we cultured primary untransduced (UTD) human macrophages alone or together with $HER2^+$ SKBR3 tumor cells. According to qPCR analysis, SLC38A2 mRNA levels were significantly diminished with tumor cell co-culture, a finding further corroborated by diminished SLC38A2 protein expression observed with immunoblotting (**Figure 3K**). In line with these results, immunofluorescence imaging confirmed decreased SLC38A2 expression in macrophages after co-culture with tumor cells (**Figure 3L**), thus supporting that the breast TME impairs glutamine transport and contributes to the metabolic aberrations observed in these cells.

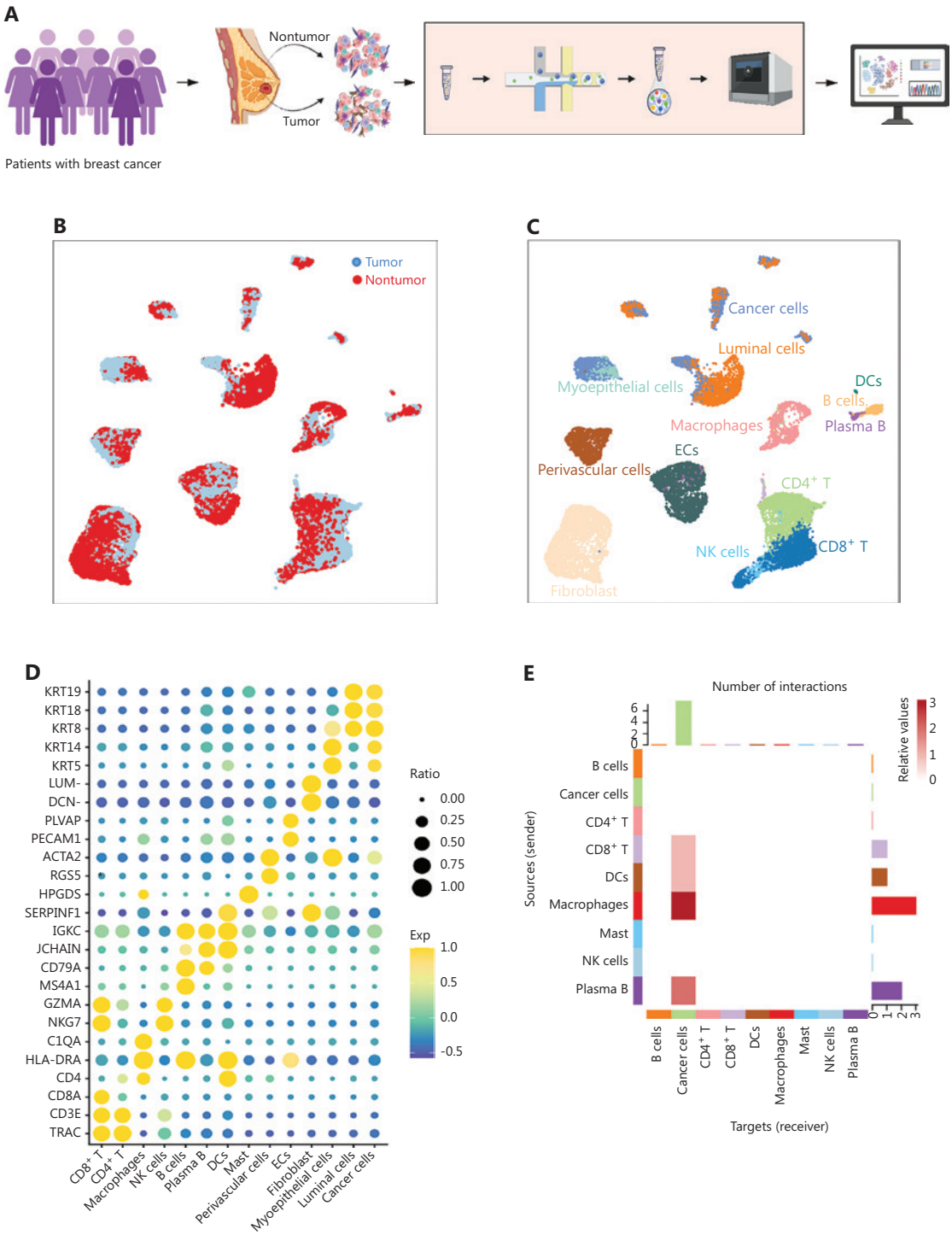


Figure 1 Continued

Engineering of SLC38A2-overexpressing CAR-Ms

Because macrophages exhibit a glutamine-restricted state associated with diminished SLC38A2 expression in the TME, we reasoned that combining metabolic enhancement with CAR-M engineering might restore the glutamine metabolic fitness of macrophages and thereby potentiate their antitumor functionality. Clinical studies have demonstrated the safety and preliminary antitumor activity of anti-HER2 CAR-Ms in

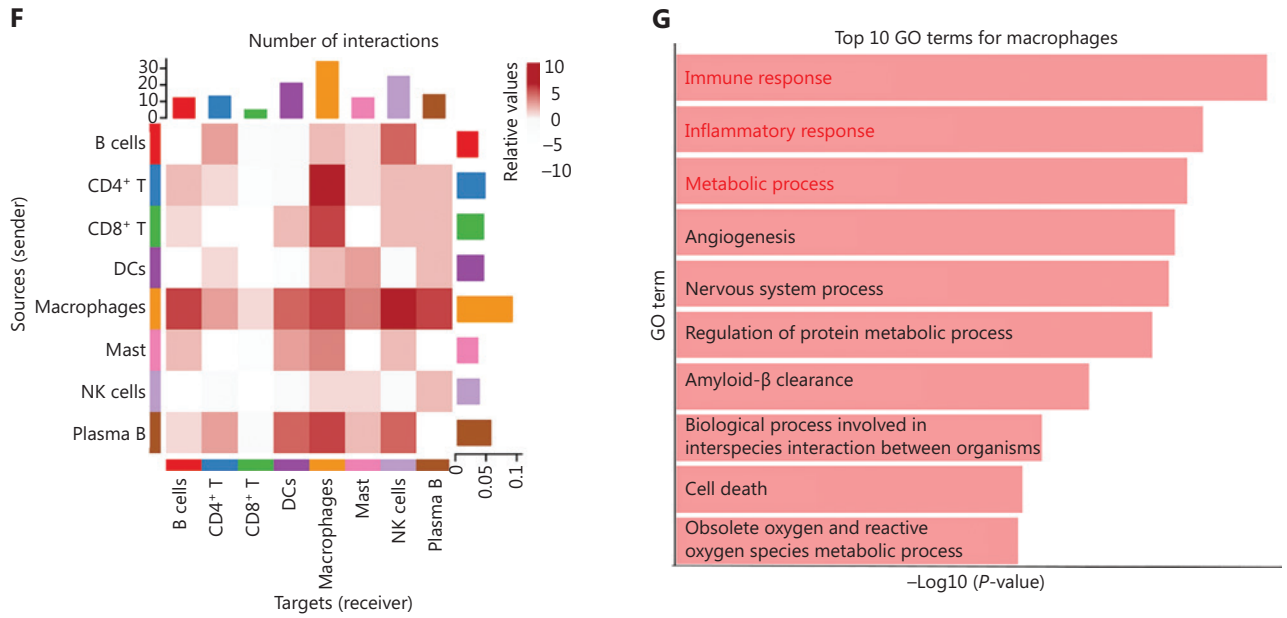


Figure 1 Single-cell transcriptome profiles in breast cancers. (A) Schematic overview of the published single-cell RNA-sequencing dataset (GSE155109), consisting of tumor and matched nontumor breast tissues collected from 9 patients with early-stage breast cancer. (B) Uniform manifold approximation and projection (UMAP) plots displaying 2 groups. (C) UMAP plots displaying major cell types. (D) Dot plot showing the expression distribution of selected canonical cell markers in major cell types. (E, F) Heatmaps depicting the number of predicted cell-cell communication between immune cells and tumor cells (E) and among immune cell subsets (F). Rows represent signal-sending cell populations (sources), and columns represent signal-receiving cell populations (targets). The bars along the top and right of each heatmap indicate the total incoming (column sum) and outgoing (row sum) signaling, respectively. (G) Top 10 gene ontology (GO) pathways notably enriched in macrophages. UMAP, uniform manifold approximation and projection; DCs, dendritic cells; ECs, endothelial cells; Plasma B, plasma B cells.

breast cancers, yet their antitumor efficacy remains suboptimal[8]. Therefore, we sought to engineer anti-HER2 CAR-Ms *via* SLC38A2 overexpression. The parental anti-HER2 CAR comprises a trastuzumab-derived HER2 scFv, CD8α hinge, 218-linker, CD28 transmembrane domain, and human CD3ζ signaling module. Building on this architecture, we incorporated a metabolic augmentation module through overexpression of SLC38A2. This SLC38A2-expressing anti-HER2 CAR (SLC38A2/anti-HER2 CAR) was successfully assembled and cloned into the pAdEasy-EF1-MCS-CMV-EGFP adenoviral vector, in which EGFP was included as a reporter gene to enable visualization and tracking of transduced macrophages (**Figure 4A and 4B**). To dissect the contributions of individual CAR modules, we also generated 2 truncated variants: (i) an intracellular-domain-only (ICD-only) construct, which retained the CD28/CD3ζ endodomain but lacked the antigen-binding ectodomain, and therefore served as a signaling-competent but ligand-independent control; and (ii) an extracellular-domain-only (ECD-only) construct, which included the HER2-specific scFv and hinge region but lacked intracellular signaling motifs, and functioned as a binding-competent yet signaling-deficient comparator. For functional benchmarking, a full-length anti-HER2 CAR-Ms, incorporating both antigen-recognition and CD3ζ-mediated signaling modules, was included in parallel. The full-length construct was verified with Sanger sequencing (**Supplementary material**).

Human macrophages were stably transduced with the above CAR constructs to generate anti-HER2 CAR-Ms and SLC38A2/anti-HER2 CAR-Ms. Macrophages transduced with an empty EGFP vector were used as controls and designated as GFP-Ms. Ad5f35-based adenoviral transduction of human macrophages resulted in high-efficiency CAR expression (**Figure 4C and 4D**). As expected, SLC38A2/anti-HER2 CAR-Ms displayed markedly elevated SLC38A2 expression, and the transporter appropriately localized to the plasma membrane (**Figure 4E–4I**). Flow cytometric analysis indicated a notable enhancement of surface SLC38A2 expression in the SLC38A2-engineered cells, and quantitative assessment of fluorescence intensity confirmed the highest surface abundance in SLC38A2/anti-HER2 CAR-Ms (**Figure 4E and 4F**). Consistently, qPCR analysis demonstrated robustly elevated SLC38A2 transcript levels, thus further verifying successful transcriptional upregulation (**Figure 4G**). To corroborate these findings at the protein level, we performed western blotting analysis, which showed a markedly strengthened SLC38A2 signal in the SLC38A2/anti-HER2 CAR-Ms. Densitometry

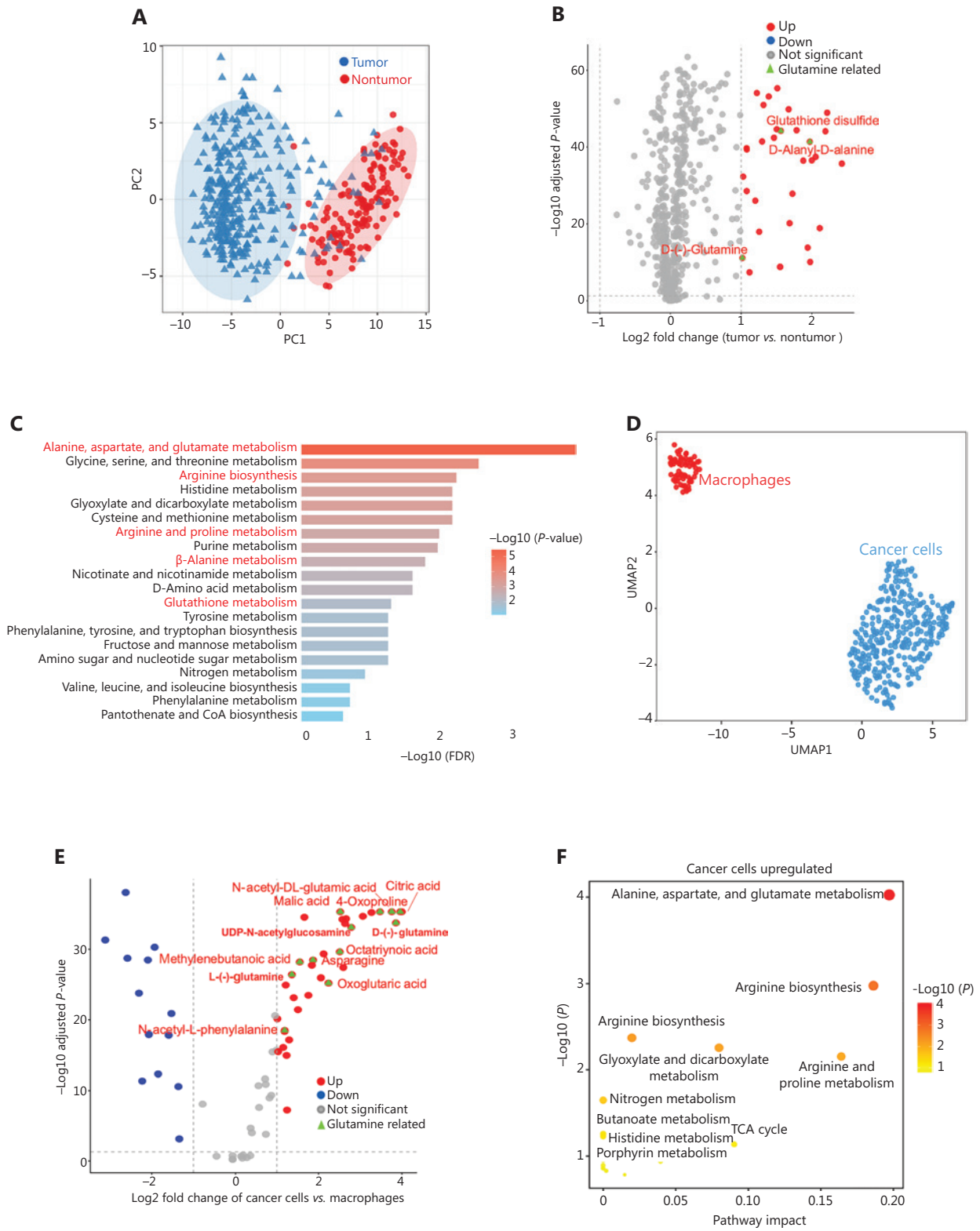


Figure 2 Continued

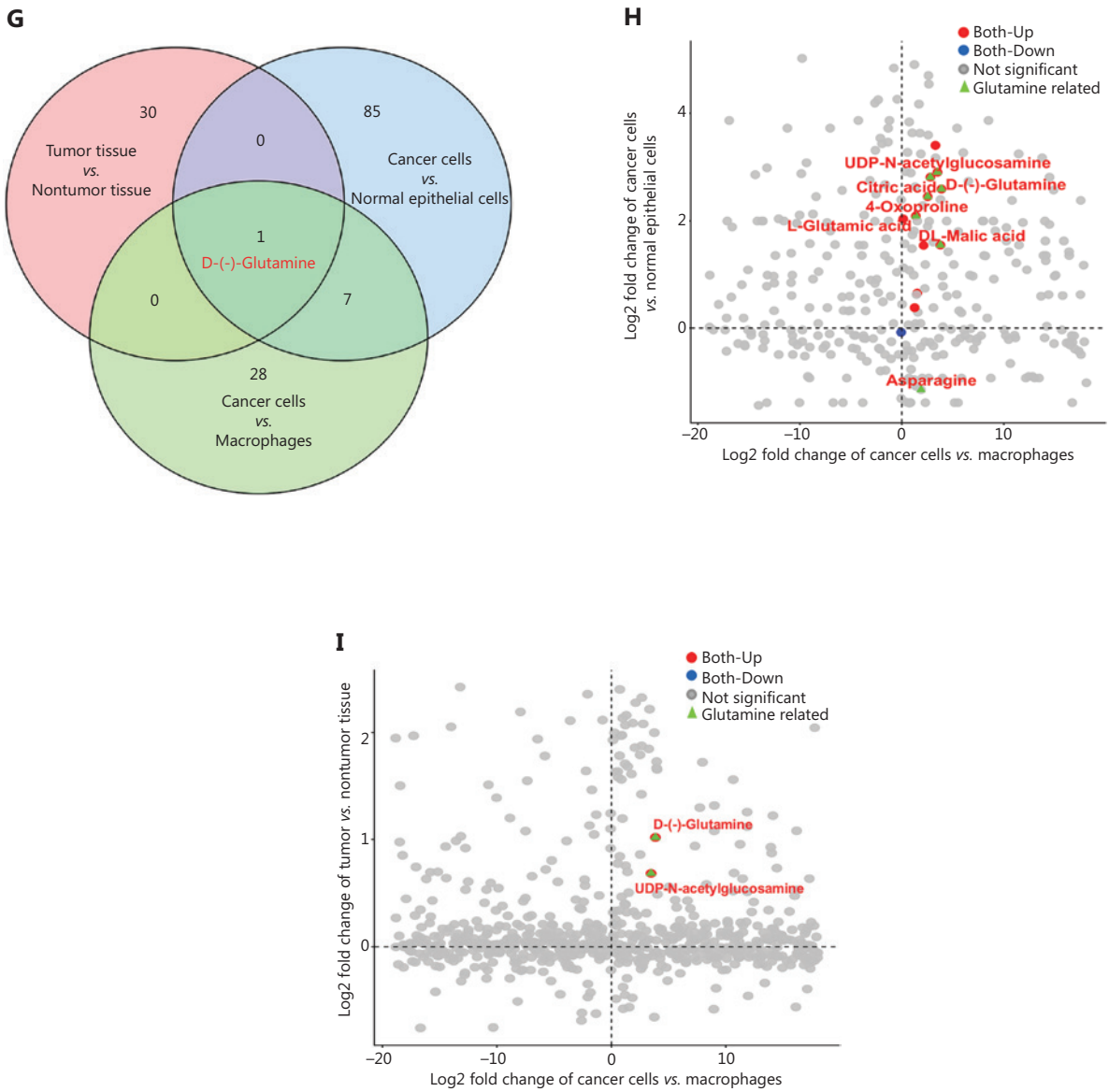


Figure 2 Integrated metabolomic analyses identifying glutamine-associated metabolic alterations in breast cancer. (A) Principal component analysis (PCA) of metabolomic profiles based on log-transformed read counts. (B) Volcano plot depicting differential metabolite abundance between groups. (C) Top 20 metabolic pathways notably enriched in all detected metabolites. (D) UMAP visualization of single-cell metabolomic profiles from macrophages and breast cancer cells. (E) Volcano plot depicting differential metabolite abundance between cancer cells and macrophages. (F) KEGG analysis of markedly upregulated pathways in breast cancer cells compared with macrophages. (G) Venn diagram showing the metabolites commonly upregulated in tumor cells across the 3 datasets: tumor *vs.* nontumor tissue, cancer cells *vs.* normal epithelial cells, and cancer cells *vs.* macrophages. (H) Dot plot illustrating fold-change differences in metabolite abundance in cancer cells *vs.* macrophages or normal epithelial cells. (I) Dot plot illustrating fold-change differences in metabolite abundance between cancer cells and macrophages, or between tumor tissues and matched normal tissues.

confirmed a clear increase in total protein abundance (**Figure 4H and 4I**). Given that the ICD-only and ECD-only constructs lacked the complete intracellular signaling modules required for full CAR assembly and surface stabilization, we performed subsequent subcellular localization analyses on only the full-length CAR-expressing cells. In agreement with the above data, confocal immunofluorescence imaging revealed a pronounced membrane-associated SLC38A2 signal in SLC38A2/anti-HER2 CAR-Ms, thereby indicating accurate transporter trafficking to the plasma membrane (**Figure 4J**).

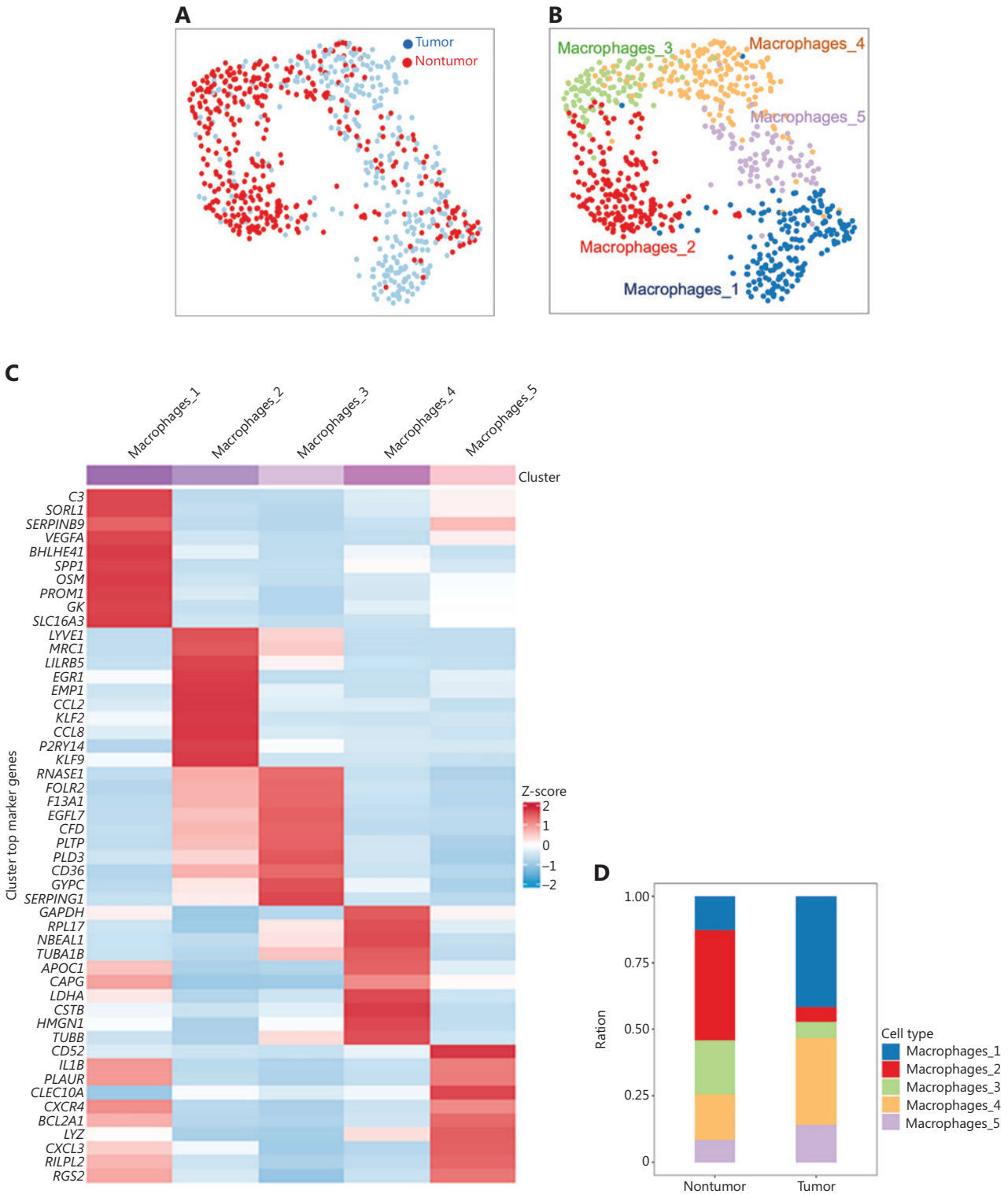


Figure 3 Continued

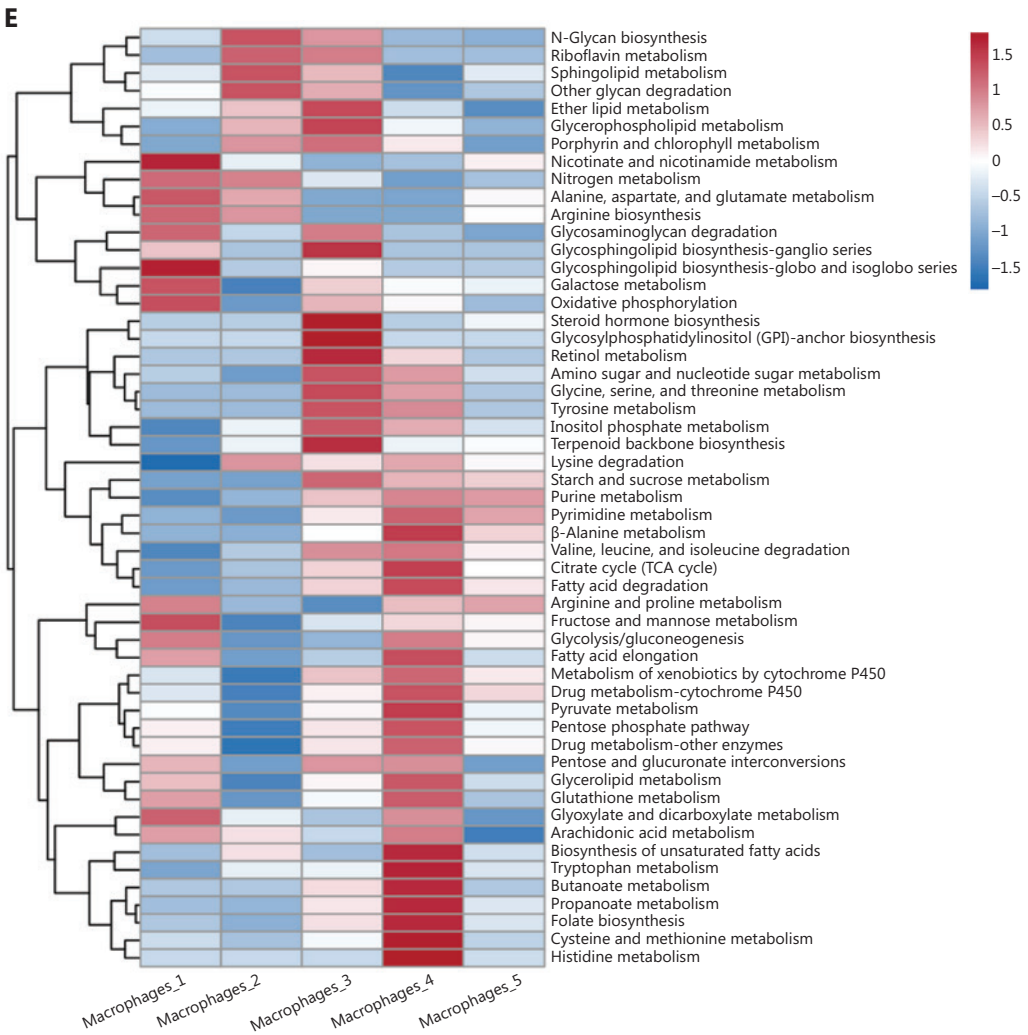


Figure 3 Continued

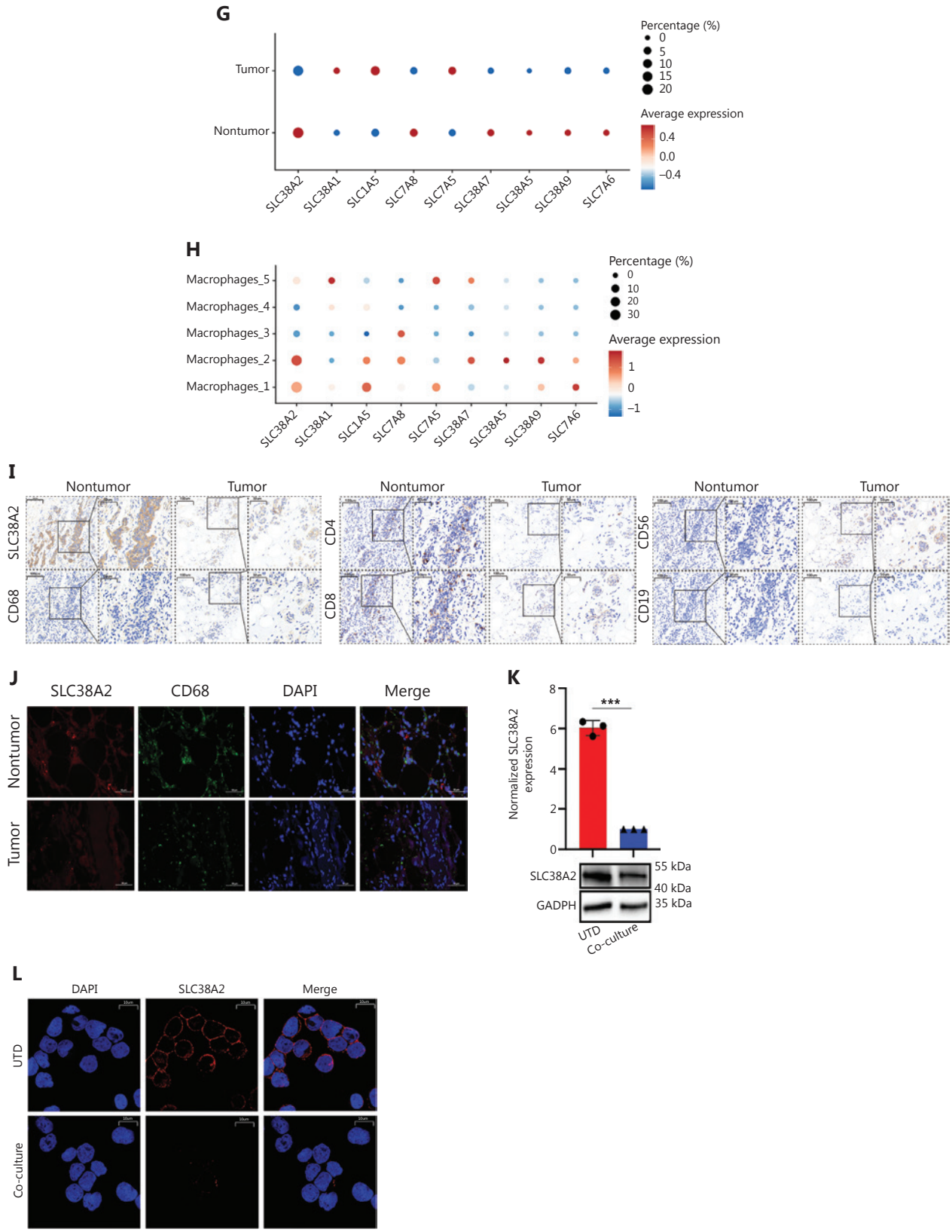


Figure 3 Comprehensive single-cell characterization of macrophage subpopulations and glutamine transporter expression in breast cancer. (A) UMAP plots displaying 2 groups. (B) UMAP plots displaying 5 cell clusters. (C) Heatmap showing expression signatures of the top 10 genes

specifically expressed in each cell cluster; the value for each gene is row-scaled. (D) Cell cluster frequency in each group. Bars are colored by cell clusters. (E) KEGG analysis indicating notably upregulated pathways in 5 cell clusters. (F) Glutamine transporters were used to annotate macrophage clusters, as shown in the UMAP visualization. (G, H) Bubble plot showing the expression of glutamine transporters across the 2 groups (G) and 5 macrophage clusters (H). (I) Representative immunohistochemical images showing SLC38A2 expression and immune cell infiltration (CD68, CD4, CD8, CD19, and CD56) in human primary breast cancer tissues, including tumor nests and adjacent nontumor regions. (J) Representative immunofluorescence staining showing SLC38A2 (red) and CD68 (green) in human primary breast cancer tissues, with nuclei counterstained with DAPI (blue). Scale bar: 50 μm. (K) Relative quantification of SLC38A2 mRNA expression in primary untransduced (UTD) human macrophages cultured alone or together with $HER2^+$ SKBR3 tumor cells for 24 h, as measured with qPCR, followed by representative immunoblots showing corresponding SLC38A2 protein expression. (L) Representative immunofluorescence images showing SLC38A2 (red) and nuclei stained with DAPI (blue) in primary untransduced (UTD) macrophages cultured alone or co-cultured with $HER2^+$ SKBR3 tumor cells for 24 h. Scale bar, 10 μm. Data are presented as mean ± SD, n = 3 per group. Statistical significance was determined with two-sided Student's t test (K). *** $P < 0.001$.

Together, these results established the successful generation of SLC38A2-augmented, HER2-targeted CAR-Ms.

Enhanced metabolic fitness and antitumor activity of SLC38A2-expressing anti-HER2 CAR-Ms

After having generated SLC38A2-augmented, HER2-targeted CAR-Ms, we next assessed whether this metabolic engineering strategy might enhance their effector functions. We first quantified glutamine-related amino acids in culture supernatants with targeted metabolomics, including glutamine, glutamate, aspartate, alanine, and arginine. Among all constructs, SLC38A2/anti-HER2 CAR-Ms exhibited the most pronounced depletion of extracellular glutamine, whereas the consumption patterns of other amino acids remained largely comparable across other constructs, including GFP-Ms, ICD-only, ECD-only, and full-length anti-HER2 CAR-Ms (**Figure 5A**). In agreement with these findings, intracellular profiling of the same glutamine-related amino acids revealed that SLC38A2/anti-HER2 CAR-Ms, compared with the other constructs, displayed the most substantial decrease in intracellular glutamine levels, whereas the levels of other amino acids were only minimally affected (**Figures 5B and S3A**). Given the selective depletion of both extracellular and intracellular glutamine in SLC38A2/anti-HER2 CAR-Ms, we next sought to determine whether enhanced glutamine consumption might be accompanied by activation of downstream glutamine metabolic pathways. To this end, we examined the expression of key enzymes involved in mitochondrial glutamine metabolism. Notably, SLC38A2/anti-HER2 CAR-Ms, compared with conventional anti-HER2 CAR-Ms and GFP-M controls, exhibited markedly greater expression of enzymes governing glutaminolysis and glutamine-derived anaplerosis, including glutaminase (GLS), glutamate dehydrogenase 1 (GLUD1), and glutamate-oxaloacetate transaminase 2 (GOT2) (**Figure 5C**).

Given that the purpose of including the ICD-only and ECD-only CAR-M constructs was to control the entire workflow of CAR-M generation, including viral transduction and *in vitro* expansion, without introducing constitutive CAR signaling, these truncated constructs served primarily as technical and structural controls rather than biologically informative comparators. Therefore, subsequent functional analyses were streamlined to the biologically relevant groups, including GFP-Ms, anti-HER2 CAR-Ms, and SLC38A2/anti-HER2 CAR-Ms, to focus on the effects of antigen-specific CAR signaling and metabolic enhancement. To determine whether this metabolic augmentation might translate into functional changes, we first examined macrophage phenotype after co-culture with $HER2^+$ SKBR3 and SKVO3 cells. Flow cytometric analysis revealed upregulation of the costimulatory ligands CD80 and CD86 on CAR-Ms, with the highest expression observed in SLC38A2/anti-HER2 CAR-Ms (**Figure 5D and 5E**), thereby indicating enhanced antigen presentation ability and an activated macrophage phenotype. Moreover, cytokine profiling revealed substantially elevated TNF-α secretion in SLC38A2/anti-HER2 CAR-Ms, accompanied by diminished levels of the immunosuppressive cytokine IL-10 (**Figure 5F**). These results indicated that SLC38A2 augmentation skewed CAR-Ms toward a proinflammatory functional state while suppressing immunoregulatory cytokine output.

To assess whether SLC38A2 overexpression might influence macrophage effector function, we co-cultured the engineered macrophages with $HER2^+$ or $HER2^-$ cancer cells at a 1:1 E:T ratio, then quantified phagocytosis by flow cytometry (**Figure 5G**). When co-cultured with $HER2^-$ cancer cells, all macrophages showed minimal and comparable engulfment, thereby indicating the absence of nonspecific phagocytic enhancement. In contrast, exposure to $HER2^+$ SKBR3 or SKVO3 cells revealed a clear functional hierarchy: SLC38A2/anti-HER2 CAR-Ms showed markedly greater phagocytic activity than GFP-Ms, and also exceeded the level achieved by the conventional anti-HER2 CAR-Ms. This augmentation built on the baseline antigen-specific activity conferred by the HER2-targeted CAR, thus reflecting an additional gain in effector function associated with SLC38A2

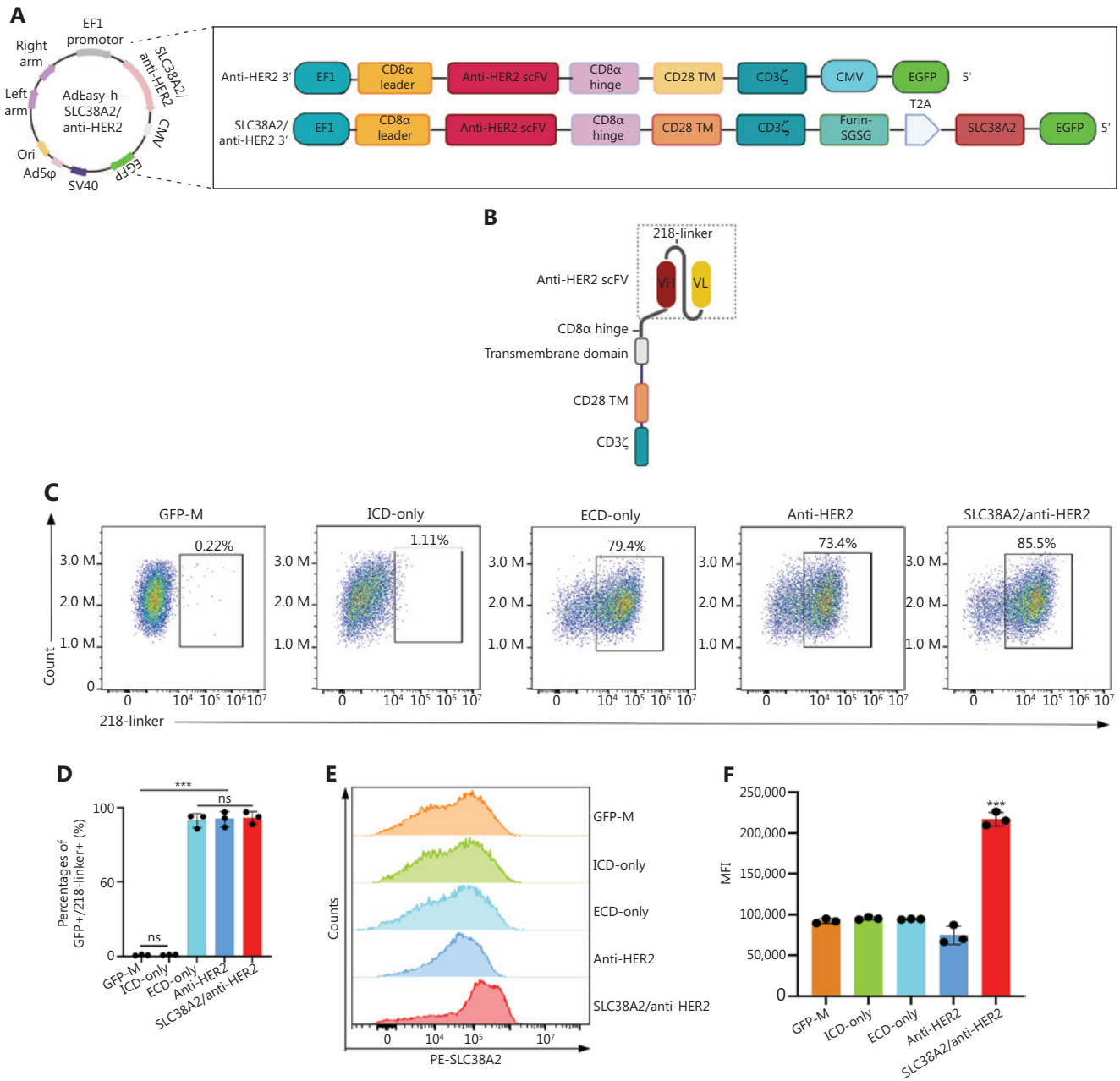


Figure 4 Continued

overexpression. In agreement with the flow cytometric results, confocal imaging further demonstrated the superior engulfment ability of SLC38A2/anti-HER2 CAR-Ms, which exhibited more internalization of HER2$^+$ tumor cells than other groups (**Figures 5H, 5I, S3B, and S3C**). Collectively, these findings demonstrated that SLC38A2-mediated metabolic augmentation not only increased glutamine acquisition but also potentiated the antigen-specific phagocytic activity of CAR-Ms.

SLC38A2 overexpression confers metabolic fitness and potentiates CAR-M antitumor immunity

To further dissect the contribution of glutamine metabolism to the enhanced phagocytic activity of SLC38A2/anti-HER2 CAR-Ms, we first evaluated their function under glutamine deprivation conditions. After 24 h of culture in glutamine-free medium, the intracellular glutamine levels in SLC38A2/

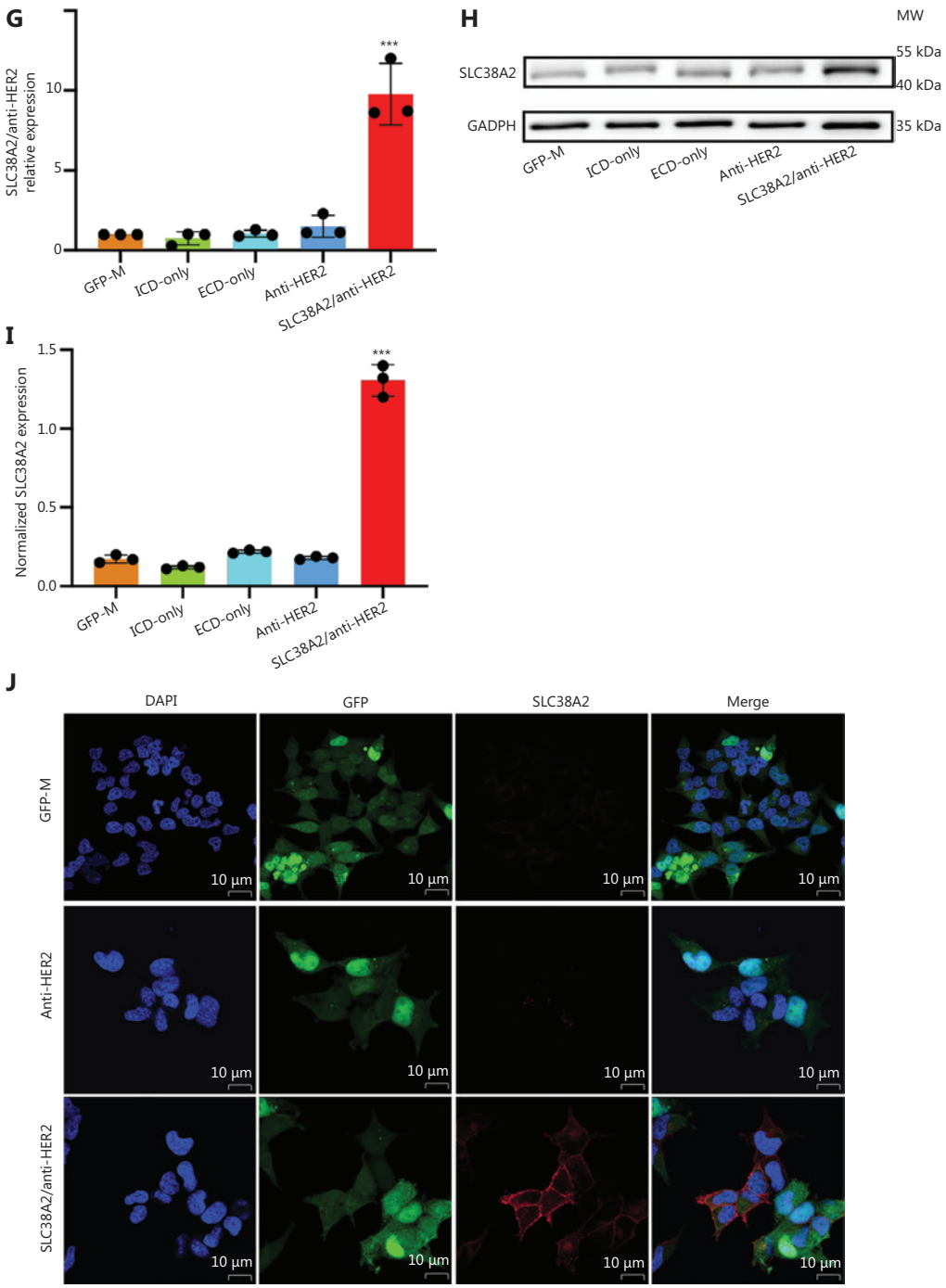


Figure 4 Engineering and characterization of SLC38A2-overexpressing CAR-macrophages. (A, B) Schematic representation of the CAR construct engineered to overexpress SLC38A2 in macrophages. (C, D) Representative flow cytometry plot showing CAR expression on adenovirus-transduced human macrophages. Percentages of 218-linker-positive cells within the gated population are indicated. (E, F) SLC38A2 expression in human macrophages (E), along with corresponding mean fluorescence intensity (MFI) values (F). (G) Relative quantification of SLC38A2 mRNA in human macrophages, measured with qPCR. (H, I) Representative immunoblots showing SLC38A2 protein expression in human macrophages (H). Quantification normalized to GAPDH and presented as fold change (I). (J) Representative immunofluorescence images showing SLC38A2 (red), GFP (green), and nuclei stained with DAPI (blue). Scale bar, 10 μm. Data are presented as mean ± SD, n = 3 per group (D, F, G, and I) and 3 biologically independent experiments in western blotting (H). Statistical significance was determined with two-sided one-way ANOVA with Tukey's test. *** $P < 0.001$, ns, not significant.

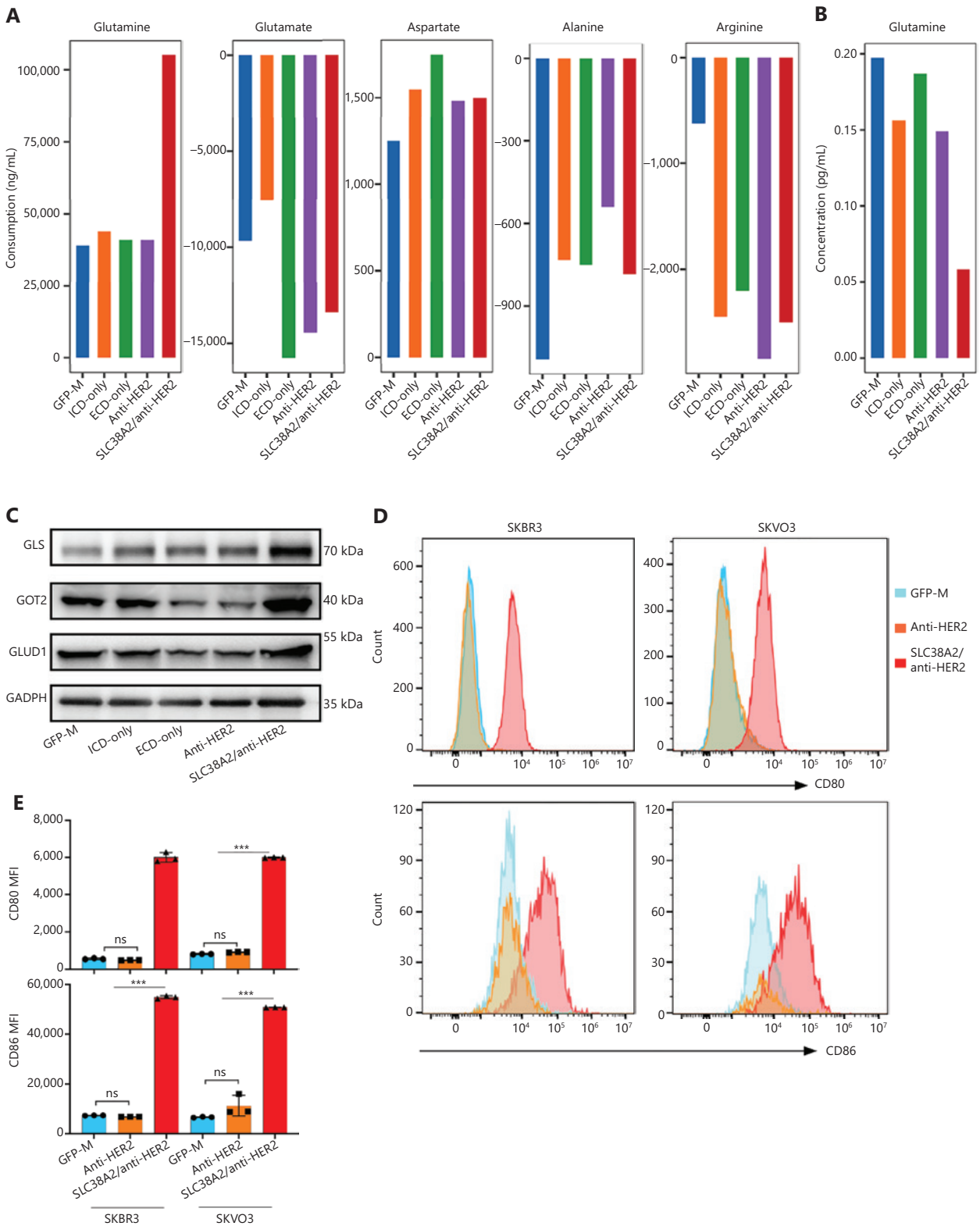


Figure 5 Continued

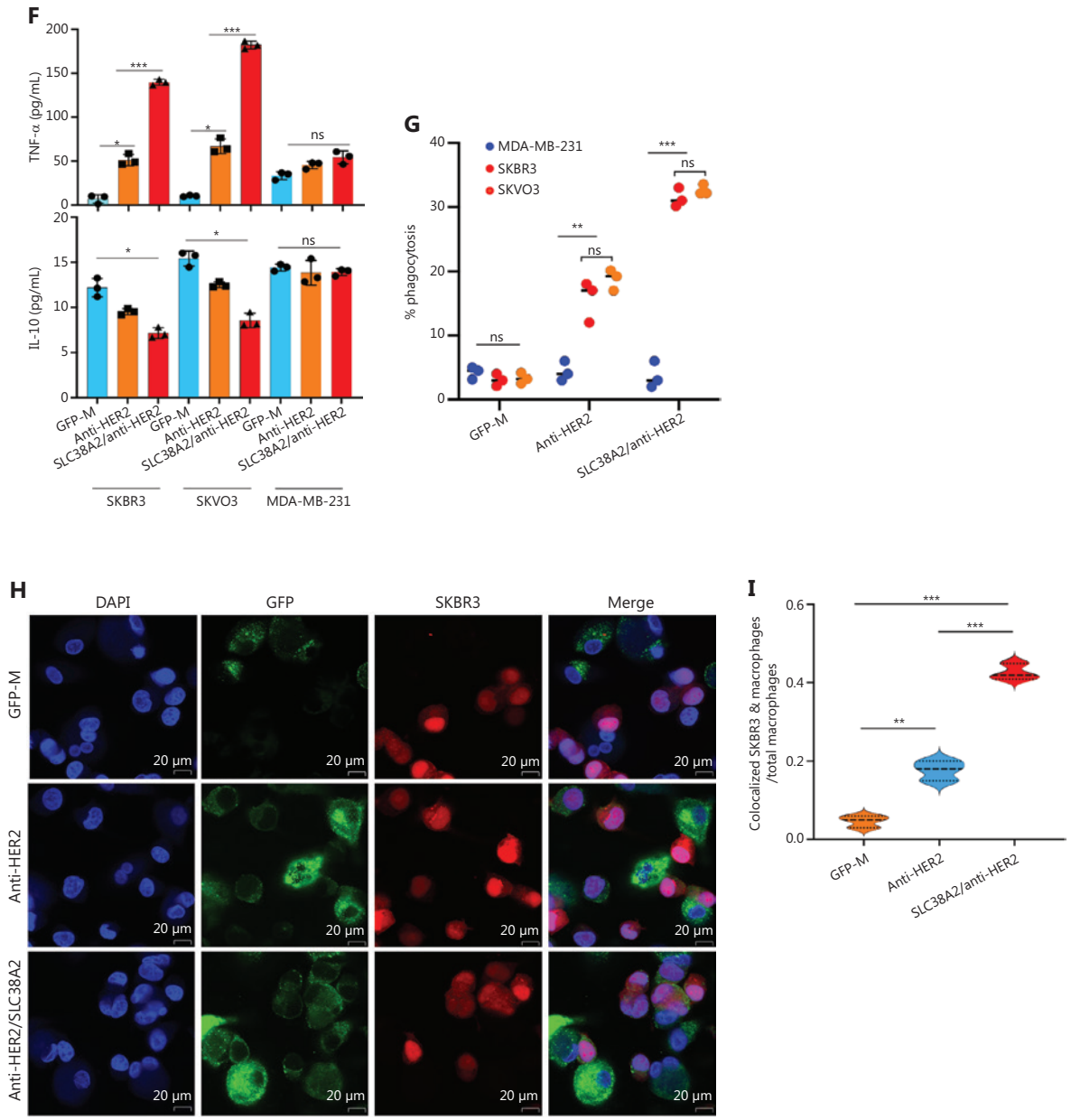


Figure 5 SLC38A2/anti-HER2 CAR-Ms enhance glutamine uptake and antigen-specific phagocytosis *in vitro*. (A, B) Targeted metabolomic analysis of glutamine-related amino acids in primary macrophages. Extracellular consumption of glutamine, glutamate, aspartate, alanine, and arginine in culture supernatants after 24 h of culture (A) and corresponding intracellular levels of glutamine in macrophages after 24 h (B). (C) Representative immunoblots of key glutamine metabolic enzymes in CAR-macrophages. (D, E) Flow cytometric analysis of macrophage activation markers CD80 and CD86 after co-culture with $HER2^+$ SKBR3 or SKOV3 cells (D), and corresponding quantification of mean fluorescence intensity (MFI) (E). (F) ELISA measurement of TNF-α and IL-10 levels in the supernatants of co-cultures of macrophages with target cells after 24 h. (G) Flow cytometry assessment of phagocytosis by GFP-Ms, anti-HER2 CAR-Ms, or SLC38A2/anti-HER2 CAR-Ms. Macrophages were co-cultured with $HER2^+$ (SKBR3 and SKVO3) or $HER2^-$ (MDA-MB-231) target cells. Data represent 3 technical replicates and are representative of at least 3 independent experiments. Statistical significance was determined with one-way ANOVA with multiple comparisons. (H, I) Representative confocal images and quantification of SKBR3 cells phagocytosed by GFP-Ms, anti-HER2 CAR-Ms, or SLC38A2/anti-HER2 CAR-Ms after 24 h co-culture. Scale bar, 20 μm. Images were acquired with an Olympus FV3000 confocal microscope and analyzed in ImageJ (H). The phagocytosis ratio was calculated as the number of colocalized SKBR3 and macrophages divided by the total number of macrophages in a single field of view (I). GLS, glutaminase; GLUD1, glutamate dehydrogenase 1; GOT2, glutamate-oxaloacetate transaminase 2. Data are presented as mean ± SD, $n = 3$ per group (E, F, G, H, and I). Statistical significance was determined with two-sided Student's *t* test (E, F, and G) and two-sided one-way ANOVA with Tukey's test (I). $^*P < 0.05$, $^{**}P < 0.01$, $^{***}P < 0.001$, ns, not significant.

anti-HER2 CAR-Ms were comparable to those observed in conventional anti-HER2 CAR-Ms (**Figure 6A**). In agreement with these findings, we detected no significant difference in phagocytosis of $HER2^+$ tumor cells, as demonstrated by representative flow cytometry analysis and confocal imaging (**Figures 6B and S4A**).

After having established that SLC38A2 overexpression enhances glutamine uptake and sustains the phagocytic activity of anti-HER2 CAR-Ms, we next sought to investigate the cellular mechanisms linking glutamine metabolic reprogramming to macrophage effector function. Given the critical roles of mitochondrial dynamics and mitochondria-mediated metabolic reprogramming in dictating immunological fate, particularly in regulating macrophage activation and phagocytic function[37-40], we examined whether SLC38A2-mediated glutamine metabolism might influence mitochondrial morphology and fission-related signaling pathways in CAR-Ms. Given that mitochondrial dynamics might integrate metabolic cues in regulating macrophage effector function, we next examined mitochondrial morphology across various CAR-M constructs. Confocal imaging revealed that mitochondria in GFP-Ms and conventional anti-HER2 CAR-Ms exhibited predominantly elongated and tubular morphologies. In contrast, SLC38A2/anti-HER2 CAR-Ms co-cultured with $HER2^+$ SKBR3 cells displayed a pronounced shift toward fragmented, punctate mitochondria, a hallmark of enhanced mitochondrial fission (**Figure 6C**). To substantiate these morphological findings, we further analyzed the expression and subcellular localization of dynamin-related protein 1 (DRP1), a key regulator of mitochondrial fission. Immunoblotting revealed greater DRP1 enrichment in the mitochondrial fraction of SLC38A2/anti-HER2 CAR-Ms than control groups, thus supporting activation of the mitochondrial fission program in these cells (**Figure 6D**). Given that effective antitumor immunity relies on coordinated interactions among multiple immune cell subsets, we next explored whether SLC38A2-engineered CAR-Ms might modulate $CD8^+$ T-cell responses. Flow cytometric analysis revealed that $CD8^+$ T cells co-cultured with SLC38A2/anti-HER2 CAR-Ms exhibited markedly enhanced proliferative ability, as indicated by elevated CFSE dilution (**Figure 6E and 6F**).

To directly assess the requirement of SLC38A2 for CAR-M function, we next used a genetic loss-of-function approach with siRNA-mediated knockdown of SLC38A2. Efficient suppression of SLC38A2 expression was confirmed by qPCR and immunoblotting (**Figure S4B**). Functionally, SLC38A2 knockdown significantly decreased glutamine uptake (**Figure 6G**) and concomitantly impaired antigen-specific phagocytic activity, as quantified by flow cytometry (**Figure 6H and 6I**). These findings further supported that sustained SLC38A2-mediated metabolic adaptation underlies the superior antitumor activity of SLC38A2/anti-HER2 CAR-Ms.

To evaluate the antitumor efficacy of SLC38A2-engineered CAR-Ms *in vivo*, we established a SKBR3 subcutaneous xenograft model and monitored tumor growth with BLI. Representative imaging showed that treatment with SLC38A2/anti-HER2 CAR-Ms, compared with controls, resulted in markedly lower tumor burden (**Figure 6J and 6K**). Therefore, SLC38A2 overexpression enhanced the *in vivo* antitumor activity of CAR-Ms, in agreement with our *in vitro* observations.

Discussion

Despite recent advances underscoring the therapeutic potential of CAR-Ms, their antitumor efficacy remains suboptimal. The TME can reprogram macrophages toward immunosuppressive phenotypes, thereby constraining the clinical utility of CAR-M therapies[12,41]. In this study, we identified glutamine as a key metabolic vulnerability in the TME and revealed SLC38A2 as a critical glutamine transporter governing macrophage glutamine uptake and metabolic fitness. Metabolically engineered SLC38A2-overexpressing CAR-Ms exhibited enhanced glutamine utilization and showed a substantial increase in antitumor activity.

CAR technology has revolutionized cancer immunotherapy. After the clinical success of CAR-T cells in hematological malignancies, CAR-M therapy has emerged as a promising next-generation strategy for solid tumors[42-44]. Recent work has also reported the generation of CAR-Ms from human pluripotent stem cells, which can be repolarized *via* innate immune activation to enhance antitumor activity[10]. This effect is largely attributable to the inherent advantages of macrophages, including their robust tumor infiltration, potent phagocytic ability, and ability to remodel the TME. Early-phase clinical trials have demonstrated favorable safety profiles and preliminary antitumor activity in patients with advanced solid tumors, thus highlighting the therapeutic potential of this modality. In recent years, substantial efforts have been devoted to optimizing CAR designs, and most engineering strategies have focused on enhancing antigen recognition and strengthening downstream activation[45-47]. However, macrophage effector functions, particularly phagocytosis, metabolic fitness, and persistence within the tumor mass, are substantially shaped by the harsh metabolic milieu of nutrient-competitive and immunosuppressive solid tumors. Traditional CAR optimization frameworks therefore fall short of addressing the unique biological requirements of macrophages in the TME. Herein, we demonstrated that selective enhancement of glutamine acquisition through forced expression of the glutamine transporter SLC38A2 substantially augmented the anti-tumor activity of HER2-targeted CAR-Ms. These findings highlight metabolic access as a previously underappreciated determinant of CAR-M functionality in solid tumors. Importantly, beyond classical CAR redesign, our work introduces a metabolism-based strategy to optimize CAR-M engineering, thus emphasizing the bifunctional CAR design integrating antigen targeting and metabolic modulation in solid tumors.

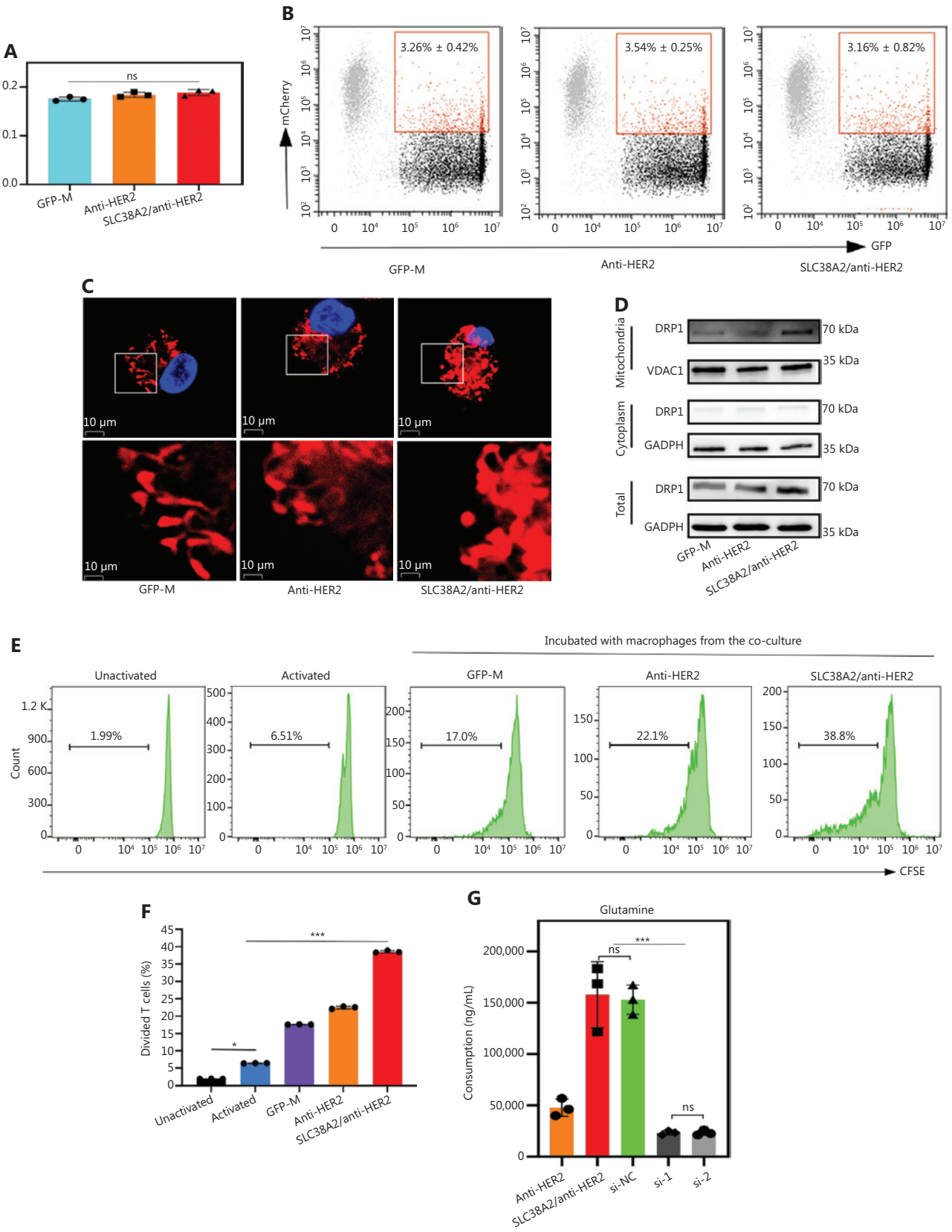


Figure 6 Continued

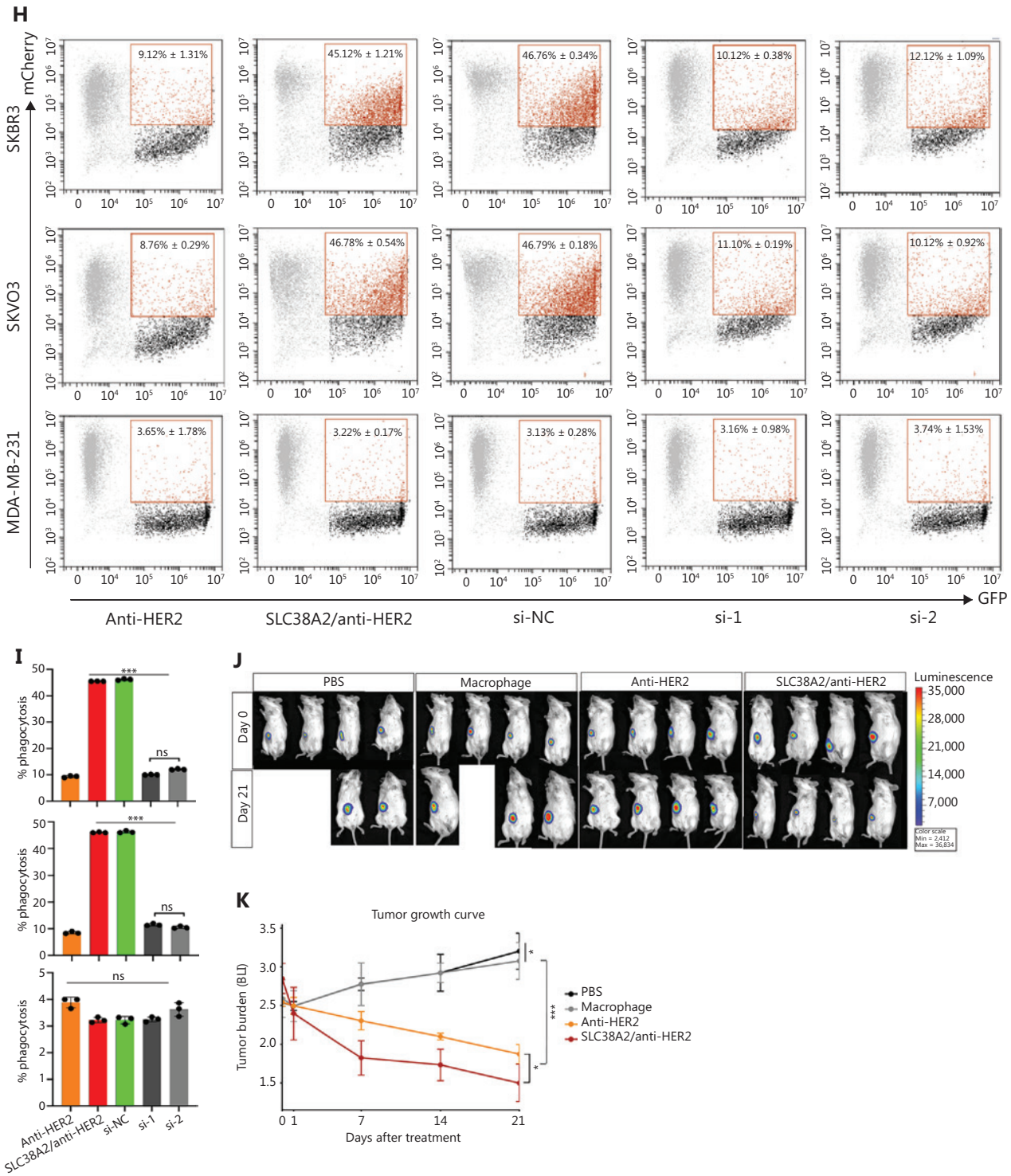


Figure 6 SLC38A2 overexpression promotes CAR-M phagocytosis, CD8 activation, and tumor suppression. (A) Targeted metabolomic analysis of intracellular glutamine levels in primary macrophages cultured under glutamine-free conditions. (B) Representative flow cytometry plots showing phagocytosis of mCherry-labeled HER2$^+$ SKVO3 tumor cells by GFP$^+$ macrophages after 24 h of co-culture in glutamine-free medium. Phagocytosis was quantified as the proportion of GFP$^+$ macrophages positive for the mCherry signal. (C) Representative immunofluorescence images showing mitochondria labeled with MitoTracker Red and nuclei stained with DAPI (blue). (D) Representative immunoblots of DRP1 in whole-cell lysates and mitochondrial and cytosolic fractions of macrophages. (E) Effects of the macrophages on T-cell proliferation,

examined with flow cytometry analysis of cell division by dilution of CFSE. (F) Quantification of proliferation of divided T cells. (G) Targeted metabolomic analysis of glutamine consumption in primary macrophages. Extracellular consumption of glutamine was measured in culture supernatants after 24 h of culture. (H) Representative flow cytometry plots showing phagocytosis of mCherry-labeled HER2$^+$ SKVO3 tumor cells by GFP$^+$ macrophages after 24 h of co-culture. (I) Quantification of phagocytosis efficiency in H. (J) Representative *in vivo* bioluminescence imaging (BLI) showing tumor growth over time in breast cancer models treated with PBS, GFP-Ms, anti-HER2 CAR-Ms, or SLC38A2/anti-HER2 CAR-Ms. (K) Quantification of BLI signals from each group (n = 4 per group). Data are presented as mean ± SD, n = 3 per group (A, B, F, G, I, and K). Statistical significance was determined with two-sided Student's t test (A and G) and two-sided one-way ANOVA with Tukey's test (F, I, and K). *P < 0.05, *** P < 0.001, ns, not significant.

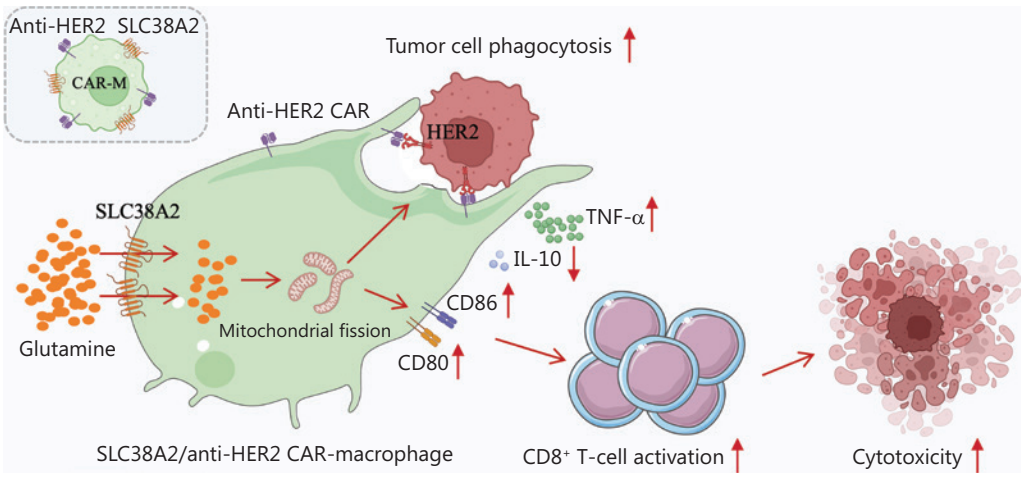


Figure 7 Schematic illustration of the proposed mechanism underlying the enhanced antitumor activity of SLC38A2/anti-HER2 CAR-engineered macrophages. Engineered macrophages overexpressing the glutamine transporter SLC38A2 and expressing a HER2-specific CAR exhibit tumor-targeted activity, thereby enabling selective recognition and binding to HER2-positive tumor cells. Upregulation of SLC38A2 increases glutamine uptake, thereby enhancing intracellular glutamine availability. Elevated intracellular glutamine promotes mitochondrial fragmentation and shifts mitochondrial dynamics toward a fission-dominant state, thereby linking glutamine metabolic reprogramming to enhanced macrophage effector function. This metabolic reprogramming supports macrophage functional activation, characterized by enhanced phagocytic ability, elevated production of pro-inflammatory cytokines such as TNF-α, diminished production of the anti-inflammatory cytokine IL-10, and upregulated expression of the co-stimulatory molecules CD80 and CD86. The augmented phagocytic activity directly enhances tumor cell clearance. Concurrently, increased CD80/CD86 expression and inflammatory cytokine secretion facilitate CD8$^+$ T-cell activation and proliferation and collectively contribute to elevated cytotoxic responses against tumor cells. CAR, chimeric antigen receptor; CAR-M, chimeric antigen receptor macrophage; SLC38A2, solute carrier family 38 member 2; TNF-α, tumor necrosis factor-alpha; IL-10, interleukin-10; CD80, cluster of differentiation 80; CD86, cluster of differentiation 86. Created with BioRender.com.

In solid tumors, nutrient scarcity and metabolic competition are critical barriers impeding immune cell effector function[29,31,37-41,48-50]. Because macrophages are more reliant on nutrients than T cells, metabolic fitness is a key determinant of CAR-M efficacy in the TME[51,52]. After activation, CAR-Ms exhibit markedly enhanced nutrient uptake and metabolite transport, which directly influence their polarization, phagocytic ability, and intratumoral persistence. Consequently, maintaining metabolic fitness has emerged as a critical factor for the therapeutic effectiveness of CAR-Ms. Activated or CAR-stimulated macrophages show elevated uptake of glutamine as key metabolites, alongside enhanced glycolysis and lipid metabolism, all of which are essential for sustaining effector functions[37,53-55]. Building on these insights, our study identified glutamine as a critical metabolite competitively utilized by macrophages and tumor cells, and highlighted its central role in shaping CAR-M functionality. Through single-cell transcriptomic profiling, we found that the glutamine transporter SLC38A2 was preferentially enriched in macrophages from normal breast tissue *vs.* TAMs, thus suggesting that glutamine acquisition physiologically relies on this transporter. Functional metabolic assays further demonstrated that CAR-Ms engineered to overexpress SLC38A2 exhibited markedly greater glutamine uptake than conventional CAR-Ms.

Importantly, these SLC38A2-overexpressing CAR-Ms maintained superior metabolic resilience under the glutamine-restricted conditions that are a hallmark of the TME. This metabolic advantage translated to markedly enhanced antigen-dependent phagocytosis and robust tumor cell clearance *in vitro*. SLC38A2-overexpressing CAR-Ms not only exhibited markedly enhanced antigen-dependent phagocytosis and reinforced metabolic ability, thereby enabling superior effector performance under glutamine-restricted conditions, but also displayed enhanced mitochondrial fission, a mechanism underlying their increased phagocytic activity (**Figure 7**). In parallel, *in vitro* assays demonstrated that SLC38A2-overexpressing CAR-Ms promoted $CD8^+$ T cell proliferation and activation. These findings highlighted the dual benefits of metabolically empowered CAR-M therapy in augmenting innate macrophage effector functions and supporting adaptive T cell responses. Importantly, these metabolic and functional enhancements translated to significant tumor growth suppression in $HER2^+$ tumor-bearing mouse models. Together, these findings delineated glutamine access as a previously underappreciated bottleneck for CAR-M performance and established a rational framework for metabolic-reprogramming-based optimization of macrophage-directed immunotherapy.

A limitation of our study is that, although we demonstrated tumor growth inhibition in HER2-positive mouse models, comprehensive *in vivo* validation across other solid tumor types remains needed to fully generalize the therapeutic potential of metabolically enhanced CAR-Ms. In addition, although we elucidated that SLC38A2-mediated glutamine uptake promoted mitochondrial fission and enhanced phagocytic activity *in vitro*, the broader metabolic mechanisms through which CAR-Ms modulate other immune cell populations within the TME remain to be fully characterized. Future studies will expand *in vivo* evaluations to additional tumor models and systematically investigate the metabolic crosstalk between CAR-Ms and the surrounding immune milieu to optimize CAR-Ms design and advance metabolism-based immunotherapy strategies.

Conclusions

Overall, this study demonstrated that metabolic engineering through enforced SLC38A2 expression restored glutamine fitness and enhanced the antitumor activity of HER2-targeted CAR-Ms in solid tumors. Increased glutamine uptake promoted mitochondrial fission and functional activation, thus improving phagocytosis and enhancing antitumor immune responses within the TME. Although further studies are needed to validate its broader applicability and long-term efficacy, our findings highlight glutamine metabolism as a key regulator of CAR-M function and provide a rational metabolic strategy to optimize macrophage-based immunotherapy in solid tumors.

Acknowledgments

We sincerely thank Professor Yu Shi [Institute of Pathology and Southwest Cancer Center, Southwest Hospital, Third Military Medical University (Army Medical University)] and Professor Jun Shen (State Key Laboratory of Experimental Hematology) for valuable scientific input and insightful discussions, which substantially contributed to the development and refinement of this study.

Grant support

This work was supported by grants from the National Key R&D Program of China (Grant Nos. 2021YFA1103000 and 2021YFA1302000), National Natural Science Foundation of China (Grant Nos. 82572106, 82125017, and 92359302), Guangdong Province Youth Top Talent Special Pillar Program 2024, Natural Science Foundation of Guangdong Province (Grant No. 2314050001076), Guangdong Basic and Applied Basic Research Foundation (Grant Nos. 2023A1515011033, 2024B1515040006, and 2025A1515012431), Guangdong Major Project of Basic Research (Grant No. 2023B0303000018), Guangzhou Science and Technology Plan Project (Grant No. 2025B03J0063), Noncommunicable Chronic Diseases–National Science and Technology Major Project (Grant No. 2025ZD0544000), Guangdong Provincial Clinical Research Center for Breast Diseases (Grant No. 2023B110005), the Science and Technology Program of Guangzhou (Grant No. 2024A04J6568), New Cornerstone Science Foundation through the New Cornerstone Investigator Program, and XPLORER PRIZE.

Conflict of interest statement

No potential conflicts of interest are disclosed.

Author contributions

Conceived and designed the analysis: Qiyi Zhao, Mingzhu Liu.
Collected the data: Mingzhu Liu, Jiang Li, Qingxi Chen, Yunxuan Zhou.
Contributed data or analysis tools: Qiyi Zhao, Junchao Cai, Jin Jin, Shicheng Su.
Performed the analysis: Luoling Zhang, Ning Wen.
Wrote the paper: Mingzhu Liu, Qiyi Zhao.

Data availability statement

The data generated in this study are available upon request from the corresponding author.

References

1. Li J, Chen P, Ma W. The next frontier in immunotherapy: potential and challenges of CAR-macrophages. Exp Hematol Oncol. 2024; 13: 76.
2. Li N, Geng S, Dong ZZ, Jin Y, Ying H, Li HW, et al. A new era of cancer immunotherapy: combining revolutionary technologies for enhanced CAR-M therapy. Mol Cancer. 2024; 23: 117.
3. Zhou X, Liu X, Huang L. Macrophage-mediated tumor cell phagocytosis: opportunity for nanomedicine intervention. Adv Funct Mater. 2021; 31: 2006220.
4. Liu T, Zhang M, Farsh T, Li H, Kishishita A, Barpanda A, et al. Exploitable mechanisms of antibody and CAR mediated macrophage cytotoxicity. Nat Commun. 2025; 16: 5616.
5. Cortés-Selva D, Dasgupta B, Singh S, Grewal IS. Innate and innate-like cells: the future of chimeric antigen receptor (CAR) cell therapy. Trends Pharmacol Sci. 2021; 42: 45-59.
6. Deng Z, Loyher PL, Lazarov T, Li L, Shen Z, Bhinder B, et al. The nuclear factor ID3 endows macrophages with a potent anti-tumour activity. Nature. 2024; 626: 864-73.
7. Kerzel T, Giacca G, Beretta S, Bresesti C, Notaro M, Scotti GM, et al. *In vivo* macrophage engineering reshapes the tumor microenvironment leading to eradication of liver metastases. Cancer Cell. 2023; 41: 1892-910.e10.
8. Reiss KA, Angelos MG, Dees EC, Yuan Y, Ueno NT, Pohlmann PR, et al. CAR-macrophage therapy for HER2-overexpressing advanced solid tumors: a phase 1 trial. Nat Med. 2025; 31: 1171-82.
9. Li X, Wang X, Wang H, Zuo D, Xu J, Feng Y, et al. A clinical study of autologous chimeric antigen receptor macrophage targeting mesothelin shows safety in ovarian cancer therapy. J Hematol Oncol. 2024; 17: 116.
10. Shen J, Lyu S, Xu Y, Zhang S, Li L, Li J, et al. Activating innate immune responses repolarizes hPSC-derived CAR macrophages to improve anti-tumor activity. Cell Stem Cell. 2024; 31: 1003-19.e1009.
11. Pierini S, Gabbasov R, Oliveira-Nunes MC, Qureshi R, Worth A, Huang S, et al. Chimeric antigen receptor macrophages (CAR-M) sensitize HER2+ solid tumors to PD1 blockade in pre-clinical models. Nat Commun. 2025; 16: 706.
12. Villanueva MT. Macrophages get a CAR. Nat Rev Drug Discov. 2020; 19: 308.
13. Sterner RC, Sterner RM. CAR-T cell therapy: current limitations and potential strategies. Blood Cancer J. 2021; 11: 69.
14. June CH, O'Connor RS, Kawalekar OU, Ghassemi S, Milone MC. CAR T cell immunotherapy for human cancer. Science. 2018; 359: 1361-5.
15. Du B, Qin J, Lin B, Zhang J, Li D, Liu M. CAR-T therapy in solid tumors. Cancer Cell. 2025; 43: 665-79.
16. Maalej KM, Merhi M, Inchakalody VP, Mestiri S, Alam M, Maccalli C, et al. CAR-cell therapy in the era of solid tumor treatment: current challenges and emerging therapeutic advances. Mol Cancer. 2023; 22: 20.
17. Liu X, Sun H, Liang J, Yu H, Xue M, Li Y, et al. Metabolic interplay between endometrial cancer and tumor-associated macrophages: lactate-induced M2 polarization enhances tumor progression. J Transl Med. 2025; 23: 923.
18. Huo Y, Zhang H, Sa L, Zheng W, He Y, Lyu H, et al. M1 polarization enhances the antitumor activity of chimeric antigen receptor macrophages in solid tumors. J Transl Med. 2023; 21: 225.
19. Duan Z, Li Z, Wang Z, Chen C, Luo Y. Chimeric antigen receptor macrophages activated through TLR4 or IFN-γ receptors suppress breast cancer growth by targeting VEGFR2. Cancer Immunol Immunother. 2023; 72: 3243-57.
20. Fu J, Zhang Y, Lv Y, Li R, Gu H, Yang J. A bioactive lipid nanoparticle integrating arachidonic acid enables high-efficiency mRNA delivery and potent CAR-macrophage engineering. Int J Mol Sci. 2025; 26: 9199.
21. Lu J, Ma Y, Li Q, Xu Y, Xue Y, Xu S. CAR macrophages: a promising novel immunotherapy for solid tumors and beyond. Biomark Res. 2024; 12: 86.
22. Chapman NM, Chi H. Metabolic rewiring and communication in cancer immunity. Cell Chem Biol. 2024; 31: 862-83.
23. Morva A, Arroyo AB, Andreeva L, Tapia-Abellán A, Luengo-Gil G. Unleashing the power of CAR-M therapy in solid tumors: a comprehensive review. Front Immunol. 2025; 16: 1615760.
24. Zeng W, Li F, Jin S, Ho PC, Liu PS, Xie X. Functional polarization of tumor-associated macrophages dictated by metabolic reprogramming. J Exp Clin Cancer Res. 2023; 42: 245.
25. Wei F, Wang D, Wei J, Tang N, Tang L, Xiong F, et al. Metabolic crosstalk in the tumor microenvironment regulates antitumor immunosuppression and immunotherapy resistance. Cell Mol Life Sci. 2021; 78: 173-93.
26. Cadenas-De Miguel S, Lucianer G, Elia I. The metabolic cross-talk between cancer and T cells. Trends Biochem Sci. 2023; 48: 597-609.
27. de Goede KE, Driessen AJM, Van den Bossche J. Metabolic cancer-macrophage crosstalk in the tumor microenvironment. Biology (Basel). 2020; 9: 380.
28. Kaymak I, Williams KS, Cantor JR, Jones RG. Immunometabolic interplay in the tumor microenvironment. Cancer Cell. 2021; 39: 28-37.
29. Fei Y, Cao X, Liu J. Nutritional competition within tumor microenvironment dictates anti-tumor immunity. Natl Sci Rev. 2024; 11: nwad277.
30. Clay R, Li K, Jin L. Metabolic signaling in the tumor microenvironment. Cancers (Basel). 2025; 17: 155.
31. Wang J, He Y, Hu F, Hu C, Sun Y, Yang K, et al. Metabolic reprogramming of immune cells in the tumor microenvironment. Int J Mol Sci. 2024; 25: 12223.
32. Zhang H, Li S, Wang D, Liu S, Xiao T, Gu W, et al. Metabolic reprogramming and immune evasion: the interplay in the tumor microenvironment. Biomark Res. 2024; 12: 96.
33. Geldhof V, de Rooij LPMH, Sokol L, Amersfoort J, De Schepper M, Rohlenova K, et al. Single cell atlas identifies lipid-processing and immunomodulatory endothelial cells in healthy and malignant breast. Nat Commun. 2022; 13: 5511.

34. Xiao Y, Ma D, Yang YS, Yang F, Ding JH, Gong Y, et al. Comprehensive metabolomics expands precision medicine for triple-negative breast cancer. Cell Res. 2022; 32: 477-90.
35. Zhang Y, Shi M, Li M, Qin S, Miao D, Bai Y. Dynamic single-cell metabolomics reveals cell-cell interaction between tumor cells and macrophages. Nat Commun. 2025; 16: 4582.
36. Guo C, You Z, Shi H, Sun Y, Du X, Palacios G, et al. SLC38A2 and glutamine signalling in cDC1s dictate anti-tumour immunity. Nature. 2023; 620: 200-8.
37. Li J, Ye Y, Liu Z, Zhang G, Dai H, Li J, et al. Macrophage mitochondrial fission improves cancer cell phagocytosis induced by therapeutic antibodies and is impaired by glutamine competition. Nat Cancer. 2022; 3: 453-70.
38. Mills EL, Kelly B, O'Neill LAJ. Mitochondria are the powerhouses of immunity. Nat Immunol. 2017; 18: 488-98.
39. Mehta MM, Weinberg SE, Chandel NS. Mitochondrial control of immunity: beyond ATP. Nat Rev Immunol. 2017; 17: 608-20.
40. Rambold AS, Pearce EL. Mitochondrial dynamics at the interface of immune cell metabolism and function. Trends Immunol. 2018; 39: 6-18.
41. Sloas C, Gill S, Klichinsky M. Engineered CAR-macrophages as adoptive immunotherapies for solid tumors. Front Immunol. 2021; 12: 783305.
42. Suchiita A, Sonkar SC. Revolutionizing immunotherapy: the next frontier in CAR T-cell engineering. Crit Rev Oncol Hematol. 2025; 211: 104751.
43. Sueangoen N, Prasongtanakij S. Emerging CAR immunotherapies: broadening therapeutic horizons beyond cancer. Clin Exp Med. 2025; 25: 274.
44. Singh AK, McGuirk JP. CAR T cells: continuation in a revolution of immunotherapy. Lancet Oncol. 2020; 21: e168-78.
45. Chen Y, Li J, Ma Y, Fang J, Yang Y, Yan L, et al. Recent advances in CAR-MSCs: the new engine of cellular immunotherapy evolution. J Hematol Oncol. 2025; 18: 92.
46. Feucht J, Sadelain M. Function and evolution of the prototypic CD28ζ and 4-1BBζ chimeric antigen receptors. Immunooncol Technol. 2020; 8: 2-11.
47. Velasco Cárdenas RM, Brandl SM, Meléndez AV, Schlaak AE, Buschky A, Peters T, et al. Harnessing CD3 diversity to optimize CAR T cells. Nat Immunol. 2023; 24: 2135-49.
48. Jiang Z, Hsu JL, Li Y, Hortobagyi GN, Hung MC. Cancer cell metabolism bolsters immunotherapy resistance by promoting an immunosuppressive tumor microenvironment. Front Oncol. 2020; 10: 1197.
49. Liang XH, Chen XY, Yan Y, Cheng AY, Lin JY, Jiang YX, et al. Targeting metabolism to enhance immunotherapy within tumor microenvironment. Acta Pharmacol Sin. 2024; 45: 2011-22.
50. Lim AR, Rathmell WK, Rathmell JC. The tumor microenvironment as a metabolic barrier to effector T cells and immunotherapy. Elife. 2020; 9: e55185.
51. Vitale I, Manic G, Coussens LM, Kroemer G, Galluzzi L. Macrophages and metabolism in the tumor microenvironment. Cell Metab. 2019; 30: 36-50.
52. Wang Y, Chen W, Wang Z, Cai S, Zhao X, Jin J, et al. Deciphering metabolic reprogramming of immune cells within the tumor microenvironment. J Transl Med. 2025; 23: 1055.
53. Xiao Y, Xu Y, Wang H, Yang F, Ding XH, Fu T, et al. HEBP2-governed glutamine competition between tumor and macrophages dictates immunotherapy efficacy in triple-negative breast cancer. Cell Metab. 2025; 37: 2030-47.e7.
54. Liu PS, Wang H, Li X, Chao T, Teav T, Christen S, et al. α-Ketoglutarate orchestrates macrophage activation through metabolic and epigenetic reprogramming. Nat Immunol. 2017; 18: 985-94.
55. He L, Weber KJ, Schilling JD. Glutamine modulates macrophage lipotoxicity. Nutrients. 2016; 8: 215.

Cite this article as: Liu M, Chen Q, Zhang L, Zhou Y, Wen N, Jin J, et al. Metabolic engineering of SLC38A2 reprograms glutamine utilization and enhances CAR-macrophage antitumor function in solid tumors. Cancer Biol Med. 2026; 23: 392-417. doi: 10.20892/j.issn.2095-3941.2025.0775